ISSN 1075-7015, Geology of Ore Deposits, 2006, Vol. 48, No. 2, pp. 108–133. © Pleiades Publishing, Inc., 2006.
Original Russian Text © E.O. Groznova, M.G. Dobrovol'skaya, V.A. Kovalenker, K.V. Davydov, V.T. Bitarov, M.V. Razin, 2006, published in Geologiya Rudnykh Mestorozhdenii, 2006, Vol. 48, No. 2, pp. 126–154.

Mineralogy and *PT* Formation Conditions of Lead–Zinc Ore at the Dzhimidon Deposit, North Ossetia

E. O. Groznova[a], M. G. Dobrovol'skaya[a], V. A. Kovalenker[a], K. V. Davydov[b], V. T. Bitarov[b], and M. V. Razin[a]

[a]*Institute of Geology of Ore Deposits, Petrography, Mineralogy, and Geochemistry, Russian Academy of Sciences, Staromonetnyi per. 35, Moscow, 119017 Russia*

[b]*Sevosgeologorazvedka Federal State Unitary Geological Enterprise, pr. Kosta 82, Vladikavkaz, 362008 Republic of North Ossetia–Alania, Russia*

Received August 10, 2005

Abstract—The mineralogy and *PT* formation conditions of the Dzhimidon Pb–Zn deposit in the Sadon ore district are considered. The deposit is localized in metamorphic rocks of the Buron Formation, which pertain to the pre-Jurassic basement (lower structural stage) and are cut through by Upper Paleozoic granitoids, and in the Lower Jurassic terrigenous sequence (upper structural stage). Orebodies as quartz–sulfide veins are mainly hosted in the metamorphic rocks. Galena, sphalerite, chalcopyrite, pyrite, pyrrhotite, and arsenopyrite are the most abundant sulfides, while quartz, carbonates, chlorite, sericite, and feldspar are gangue minerals. The bismuth mineralization identified at this deposit for the first time is represented by diverse phases of the Ag–Pb–Bi–S system. Five stages of the ore deposit formation are recognized: a premineral stage (quartz–feldspar), three ore-bearing stages (pyrite–arsenopyrite, pyrrhotite–chalcopyrite–sphalerite, and arsenopyrite–sphalerite–galena), and a postmineral stage (quartz–calcite); each stage comprises one or several mineral assemblages. The study of fluid inclusions in quartz, calcite, and sphalerite of the premineral, ore-forming, and postmineral stages has shown that the ore was deposited mainly from Na chloride solution with a salinity varying from >22 to <1.0 wt % NaCl equiv at a temperature from 460 to ~120°C and 430–290 bars pressure. The third stage was characterized by an abrupt increase in temperature and by the appearance of Mg(Fe,Ca) chloride solutions equally with Na chloride fluids, presumably owing to the emplacement of granite porphyry.

DOI: 10.1134/S1075701506020024

INTRODUCTION

Numerous Pb–Zn deposits (Sadon, Verkhnii and Nizhnii Zgid, Arkhon, Kholst, and others) have been known in the Sadon ore district, North Ossetia (Fig. 1) for more than 150 years.

Extensive geological exploration of this district, combined with geological mapping on various scales and specialized geophysical surveying and geochemical exploration of the adjacent areas, was conducted in the last century. These works were aimed at providing the Electrotsink plant in Vladikavkaz with ore. During this period, geologists managed to establish the main metallogenic features of the region and particular deposits therein (Vardanyants, 1935; Chernitsyn, 1985); to provide insights into the geological and structural conditions of the ore localization (Gurbanov and Zembatov, 1978; Konstantinov, 1971; Nekrasov, 1980; Bashkina, 2002); and to determine the composition, zoning, and genesis of ore mineralization (Zlatogurskaya, 1958; Prokopenko, 1958; Sorokin, 1958; Chernopyatov, 1958; Khetagurov and Katova, 1972; Granovsky, 1982; Davydov and Granovsky, 1985; Dobrovol'skaya, 1987, 1989; Lyakhov et al., 1994).

Corresponding author: E.O. Groznova. E-mail: geo@igem.ru

The forecasting of the hidden mineralization was of great importance to the Sadon ore district (Azhgirei, 1958; Zlatogurskaya, 1960; Konstantinov, 1971; Konstantinov et al., 2003). Azhgirei (1958) suggested that the hidden deposits are controlled by transverse dislocations and regarded the Dzhimidon area at the eastern plunge of the anticline as the most promising target. Konstantinov (1971) considered the contact zone between Paleozoic granitoids and overlying volcanic sequences as favorable for localization of Pb–Zn mineralization, including hidden orebodies.

The expansion of prospects of the ore district at the expense of hidden ore mineralization was confirmed by further geological exploration. In particular, the blind Yuzhny vein was found at the eastern flank of the Arkhon deposit in the early 1960s, while the hidden Bozang zone of high-grade Pb–Zn ore was discovered in the Dzhimidon ore field in the mid-1980s.

The Bozang, Tsagarsar, and East Dzhimidon ore zones are presently known within the Dzhimidon deposit. The Bozang ore zone is the reference hidden ore object in the Sadon district. The study of the geology, orebody morphology, geochemical halos, wall rock alteration, and ore composition in the Bozang

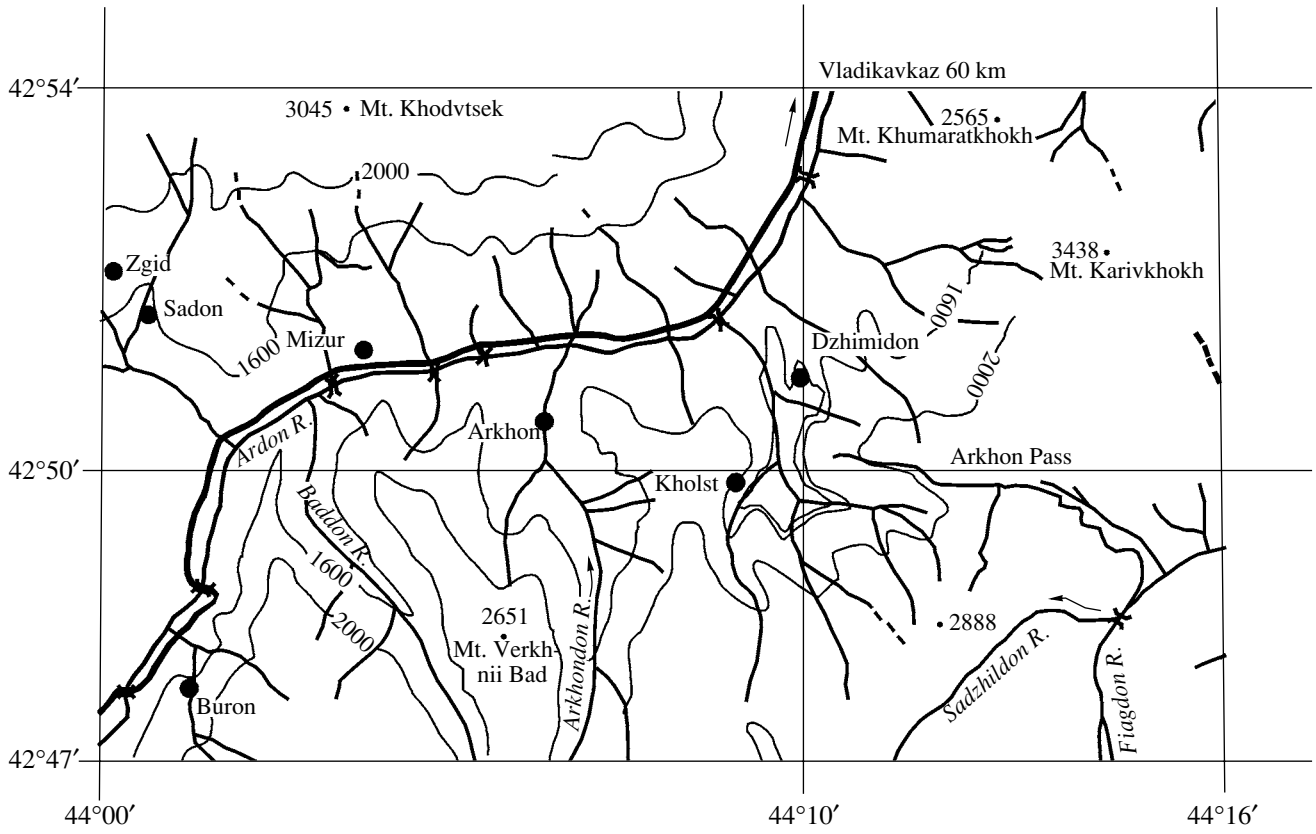

Fig. 1. Index map of the Sadon ore district. Filled circles are deposits of the Sadon ore district.

zone allowed Konstantinov et al. (2003, 2004) to propose geological–structural, geochemical, mineralogical, and geophysical criteria for forecasting, prospecting, and evaluation of hidden Pb–Zn mineralization in the Sadon ore district.

However, no detailed information on the mineralogy, geochemistry, and *PT* conditions of ore formation at the Dzhimidon deposit has been available to date. We have filled this gap, reporting new mineralogical, geochemical, and physicochemical data obtained with modern microscopic and analytical methods.

BRIEF GEOLOGICAL CHARACTERIZATION OF THE SADON ORE DISTRICT AND THE DZHIMIDON DEPOSIT

The geology of the Sadon ore district and particular deposits therein has been considered in numerous publications. The district is located on the northern slope of the Greater Caucasus between the axial horst anticlinorium and the Dar'yal–Bogos Rise (Nekrasov, 1980; Davydov and Granovsky, 1985; Konstantinov et al., 2003), including the Sadon–Unal Horst-Anticline, which controls the main economic deposits of the district. In cross section, this structural feature is an asymmetric fold with Upper Paleozoic granites and crystalline schists in the core and Lower Jurassic volcanosedimentary rocks at its limbs. The southern limb is gently dipping, while the northern limb dips steeply and is locally overturned northward. Both limbs are complicated by faults. Transverse faults divide the anticline into block segments. According to Konstantinov et al. (2003, 2004), the Pb–Zn deposits are controlled by transverse faults extending in a nearly N–S direction. The economic ore mineralization that typically fills shear fractures is traced to a depth of 0.5–1 km, reaching a depth of 1.5 km at the Sadon deposit.

The Dzhimidon deposit is located in the easternmost block segment of the Sadon–Unal Horst-Anticline, known as the Dzhimidon Uplift. Two structural stages are recognized at the deposit (Fig. 2). The lower stage is made up of the metamorphic rocks of the Upper Proterozoic–Lower Paleozoic Buron Formation cut through by Upper Paleozoic granites. The hornblende amphibolites at the base of the Buron Formation are gradually replaced upsection by diverse crystalline schists. The crystalline basement is overlain, with basal conglomerates at the base, by Lower Triassic terrigenous rocks of the upper structural stage. Jurassic igneous rocks, abundant at the deposit, make up a volcanic–

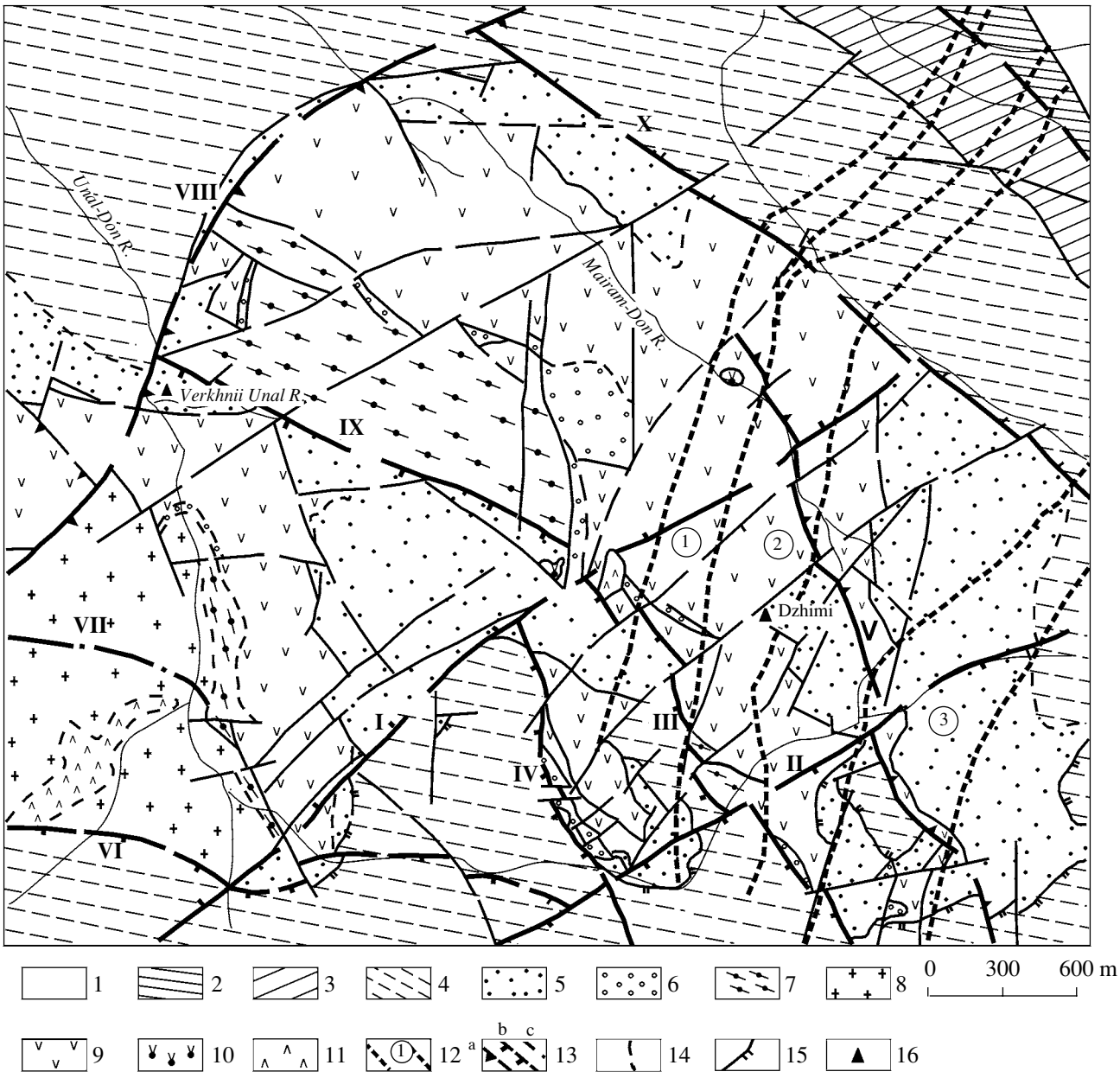

Fig. 2. Schematic geological map of the Dzhimidon ore field after K.V. Davydov. (1–6) Lower and Middle Jurassic sedimentary rocks: (1) limestone and dolomite, (2) sandstone, siltstone, clay, and limestone, (3) mudstone with sandstone interbeds, (4) shale and siltstone with sandstone interbeds, (5) sandstone and siltstone, (6) conglomerate; (7) Neoproterozoic–Lower Paleozoic Buron Formation: crystalline schists and amphibolites; (8) Late Paleozoic coarse-grained granite; (9–11) Early–Middle Jurassic volcanic–plutonic association: (9) andesitic lavas and tuffs, (10) trachyandesite, (11) andesite; (12) ore zones (numerals in circles): (1) Bozang, (2) Tsagarsar, (3) East Dzhimidon; (13) faults: (a) reverse, (b) normal, (c) faults denoted by Roman numerals in the figure: (I) First transverse, (II) Second transverse, (III) East Dzhimidon, (IV) West Dzhimidon, (V) Agshartyrag, (VI) Sadon–Unal, (VII) Latitudinal, (VIII) Tsamadon, (IX) Tsagadon, (X) Dagom ((I–IV) are normal faults and (V–X) are reverse faults); (14) inferred geological boundaries; (15) overthrusts; (16) settlements.

plutonic association that comprises andesitic rocks of the volcanic Ossetia Complex and subvolcanic and hypabyssal diorite, granite porphyry, and trachyandesite intrusions of the Ardon–Nogkau Complex (Fig. 2). The igneous rocks underwent hydrothermal quartz–sericite and calcite–chlorite–quartz alteration.

The Dzhimidon Uplift has a relatively simple anticlinal structure. A series of transverse faults divides it into separate blocks. The ore mineralization is mainly controlled by the transverse West and East Dzhimidon faults (Fig. 2). Premineral shear and crush zones were formed in the block bounded by these faults. The ore is

confined to tension cracks and shear fractures. On passing into the upper structural stage, the orebodies are transformed into zones of disperse silicification and chloritization accompanied by disseminated sulfides. The economic ore mineralization at the Dzhimidon deposit is constrained from below by the contact zone between the Buron amphibolites and crystalline schists, which are cut by Jurassic granitoids, whereas other deposits of the Sadon district are localized either in granite (Verkhnii Zgid, Sadon, etc.) or in volcanic and terrigenous rocks of the upper structural stage (Arkhon, Levoberezhny, etc.).

Most authors (Davydov and Granovsky, 1985; Bashkina, 2002; Konstantinov et al., 2003) point out that the orebody morphology at the Dzhimidon and other deposits of the Sadon ore field is controlled by premineral fissures and the mechanical properties of the host rocks. Sheetlike vein orebodies from a few to 200 m thick and as long as 300 m downdip (Fig. 3) are predominant and are typically accompanied by halos of stringer–disseminated ore mineralization. The present-day position of the orebodies strongly depends on post-mineral displacements, which widely vary in amplitude, from tenths of a meter to 3–40 m.

The wall rock alteration is expressed in silicification, sericitization, chloritization, and pyritization. The total thickness of metasomatic rocks replacing amphibolites attains 3–5 m. The Bozang ore zone occasionally contains feldspar and quartz–feldspar veinlets with epidote–zoisite minerals and relics of skarnoids partially replaced by sulfides (Konstantinov et al., 2004).

RESEARCH METHODS

A representative collection of samples taken during detailed mapping of the underground workings (adits 3, 8, and 47) and documentation of borehole cores (holes 061a, 0.76, 0.47, and others) was used to study the ore mineralogy and geochemistry at the Dzhimidon deposit.

The composition, structure, and texture of ore and the sequence of mineral formation were established by macroscopic and microscopic investigations of hand specimens and polished and thin sections. The laboratory studies were carried out at the Institute of Geology of Ore Deposits, Petrography, Mineralogy, and Geochemistry (IGEM), Russian Academy of Sciences (RAS).

Minerals were analyzed on a Camebax SX-50 microprobe (analyst A.I. Tsepin) at an accelerating voltage of 20 kV, an ion current of 20 nA, and a counting time of 10 s. The following standards were used: PbS (PbM_α), metallic Bi (BiM_α), metallic Ag (AgL_α), CdSe (SeL_α), FeS_2 (FeK_α and SK_α), AsGa (AsL_α), metallic Cu (CuL_α), Sb_2S_3 (SbL_α), ZnS (ZnL_α), $MnTiO_3$ (MnK_α), and metallic Cd (CdL_α). The measured relative intensities were recalculated into concentrations with the microprobe program PAP. Intergrowths of minerals and their compositions were additionally studied on a JSM 5300 SEM equipped with a LINK ISIS EDS (analyst N.V. Trubkin); the detection limit is 0.4 wt %.

The ore was analyzed with XRF on a Philips PW 2400 sequential spectrometer (analyst A.I. Yakushev). The results of measurements were processed with the Philips Super Q 2001 software package. A set of the branch reference samples of Pb–Zn sulfide ores and the State reference samples of rocks were used as standards. The detection limit for silicate matrix was 0.01 wt % in oxide form.

Major and trace ore elements in ores and sulfide concentrates were determined with INAA at the Laboratory of Radiogeology and Radioecology of IGEM RAS (analyst A.L. Kerzin).

The microthermometric study of fluid inclusions in minerals was performed on a Linkam THMSG-600 thermostage (United Kingdom) using an Olympus 80× high-resolution long-focus objective (Japan). This equipment allows recording of phase transformations in inclusions less than 5 μm in size. The investigations were conducted within the temperature range from –196 to +600°C with a measurement accuracy of ±0.2°C in the temperature interval from +60 to –60°C and with an accuracy of ±1.5…2°C beyond this range.

The homogenization temperature (T_{hom}) of two-phase inclusions was determined by the gas–solution transition point. Since the values were not corrected for pressure, the obtained T_{hom} corresponds to the minimum temperature of the mineral formation. The composition and salinity of the solutions were studied by cryometry. The salt composition of the solutions was determined by the eutectic temperature (T_{eut}), and their salinity (wt % NaCl equiv), by the melting temperatures of ice (T_{melt}) and CO_2 clathrates (T_{cl}) (Bodnar and Vityk, 1994). The measurements were performed for inclusions with identical phase proportions to avoid errors related to the necking down of vacuoles after fluid unmixing (Roedder, 1984).

The pressure was calculated for syngenetic CO_2–CH_4 and aqueous–salt inclusions (Kalyuzhny, 1982). Diagrams (Thiery, 1994) and the program FLINCOR (Brown, 1989) were used for this purpose.

MINERAL AND CHEMICAL COMPOSITION OF ORE

All researchers of Pb–Zn deposits in the Sadon ore district (G.I. Bocharova, M.G. Dobrovol'skaya, I.P. Zlatogurskaya, N.M. Prokopenko, M.S. Sakharova, V.I. Sorokin, S.F. Chernopyatov, etc.) have described a relatively simple ore mineralogy. According to the available data, the ore from all deposits is composed of the same assemblages of ore and gangue minerals, although their proportions vary from deposit to deposit and even between orebodies at the same deposit (Dobrovol'skaya, 1989). The preliminary information on the ore composition at the Dzhimidon deposit was

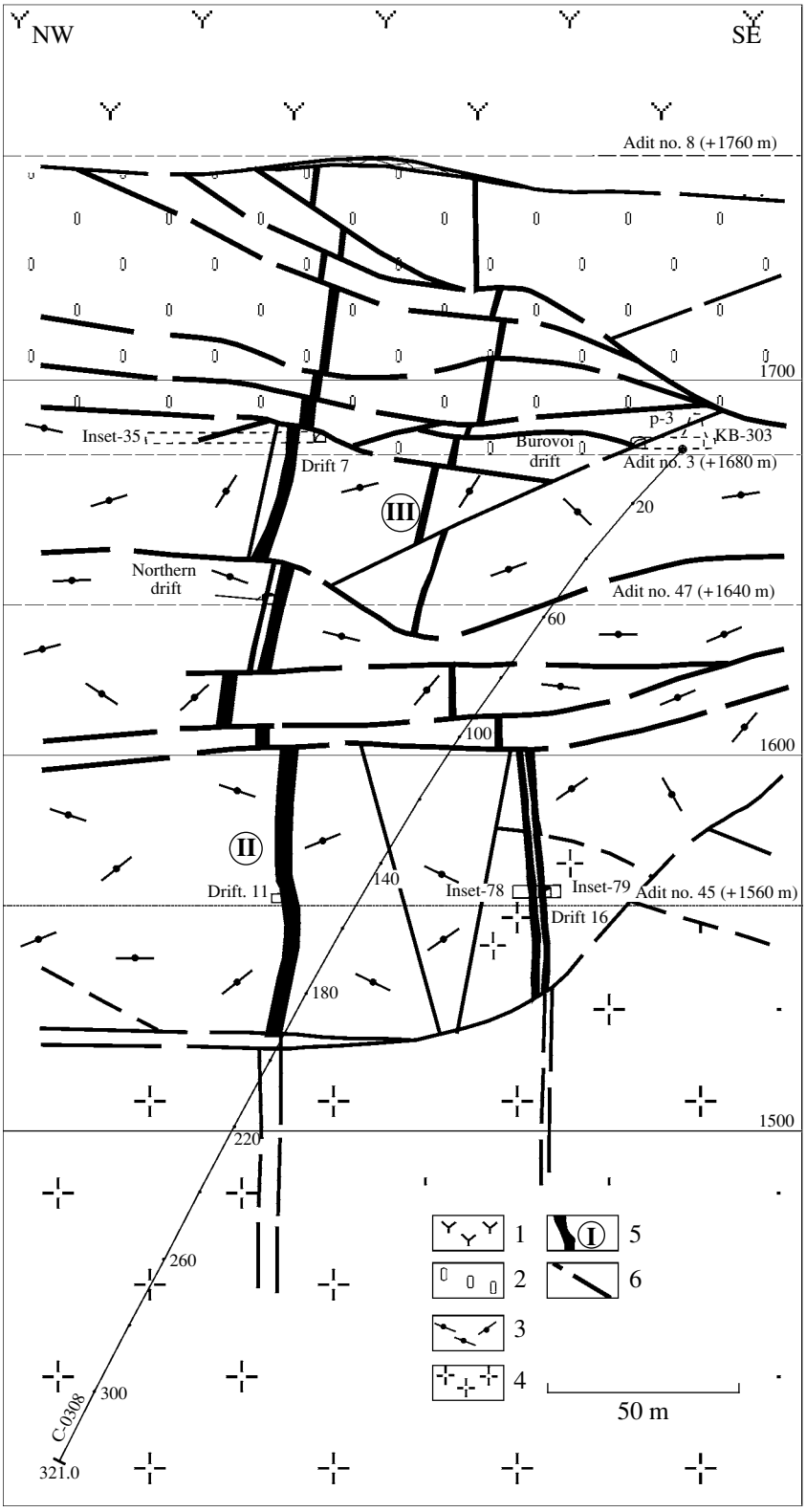

Fig. 3. Vertical section across the main orebodies of the Bozang zone, after K.V. Davydov. (1) Early Jurassic Ossetia volcanic complex: andesitic lavas and tuffs; (2) Lower Jurassic conglomerate; (3) Neoproterozoic–Lower Paleozoic Buron Formation: crystalline schists and amphibolites; (4) Middle Jurassic granite porphyry; (5) orebodies: (I) Main, (II) Central, (III) Eastern apophysis; (6) faults.

Table 1. Ore minerals at the Dzhimidon deposit

Major	Minor	Accessory
Ore minerals		
Pyrite	Pyrrhotite	Acanthite (Ag_2S)*
Galena	Magnetite	Bursaite ($Pb_5Bi_4S_{11}$)*
Sphalerite	Marcasite	Weibullite ($Pb_3Bi_4S_9$)*
Chalcopyrite		Native Bi*
Arsenopyrite		Bismuthinite (Bi_2S_3)*
		Cosalite ($Pb_2Bi_2S_5$)*
		Galenobismutite ($PbBi_2S_4$)*
		Native Ag*
		Phase $Ag_3Pb_8Bi_{11}S_{26}$*
		Phase $Pb_5Bi_2S_8$*
		Phase $Pb_4Bi_2S_7$*
		Phase Bi_2S_2*
		Fahlore
		Scheelite
		Wolframite
		Hematite
Gangue minerals		
Quartz	Dolomite	Barite
Calcite	Sericite	Microcline
	Chlorite	Knebelite*
		Fluorite

* Minerals identified in the ore for the first time.

consistent with this statement. However, the new data allowed us to characterize the mineralogy and geochemistry of the ore in more detail.

As at other deposits of the Sadon district, sphalerite, galena, pyrite, arsenopyrite, pyrrhotite, and chalcopyrite are the most abundant ore minerals at the Dzhimidon deposit. Marcasite and magnetite are second in abundance, and scheelite, wolframite, and hematite are minor minerals. Diverse bismuth sulfosalts (including previously unknown phases) and silver minerals were identified for the first time in the East Dzhimidon and Bozang ore zones. Quartz and various carbonates, including Mn-bearing varieties; barite; chlorite; sericite; and feldspar are gangue minerals, as well as Mn-knebelite, a rare olivine variety, which was identified for the first time in ore of the Dzhimidon deposit (Table 1).

Ore Minerals at the Dzhimidon Deposit

The ore-forming minerals, their intergrowths, and data on their compositional variations during mineral formation are characterized in this section.

Sphalerite as inequigranular aggregates with numerous chalcopyrite inclusions is widespread in the orebodies (Fig. 4). In some veinlets and aggregates, sphalerite is devoid of visible chalcopyrite inclusions but contains quartz, pyrrhotite, and galena grains (Fig. 4a). This probably testifies to the later crystallization of sphalerite without chalcopyrite impurities.

Chalcopyrite inclusions in sphalerite are various in shape: rounded, dotty, euhedral, skeletal, threadlike, etc. (Figs. 4b, 4c). They vary in size from submicroscopic (dustlike) to 1–2 mm in diameter. The amount of chalcopyrite inclusions often reaches 40% of the sphalerite grain area. The inclusions are distributed chaotically or related to cleavage planes, twin sutures, dislocations, crystal defects, and grain boundaries. In the central parts of sphalerite aggregates, the chalcopyrite inclusions are often enlarged and segregated. The detailed microscopic examination of chalcopyrite inclusions in sphalerite showed their different origin. They could have arisen as a result of (1) replacement of sphalerite, (2) exsolution of initially homogeneous solid solutions with subsequent redistribution and enlargement of products, and/or (3) joint crystallization of copper and zinc sulfides. The nature of chalcopyrite "disease" of sphalerite in the ore at the Dzhimidon and other deposits of nonferrous and noble metals has been previously described (Bortnikov et al., 1991). Under etching in aqua regia (HNO_3 + HCl) vapor, some grains

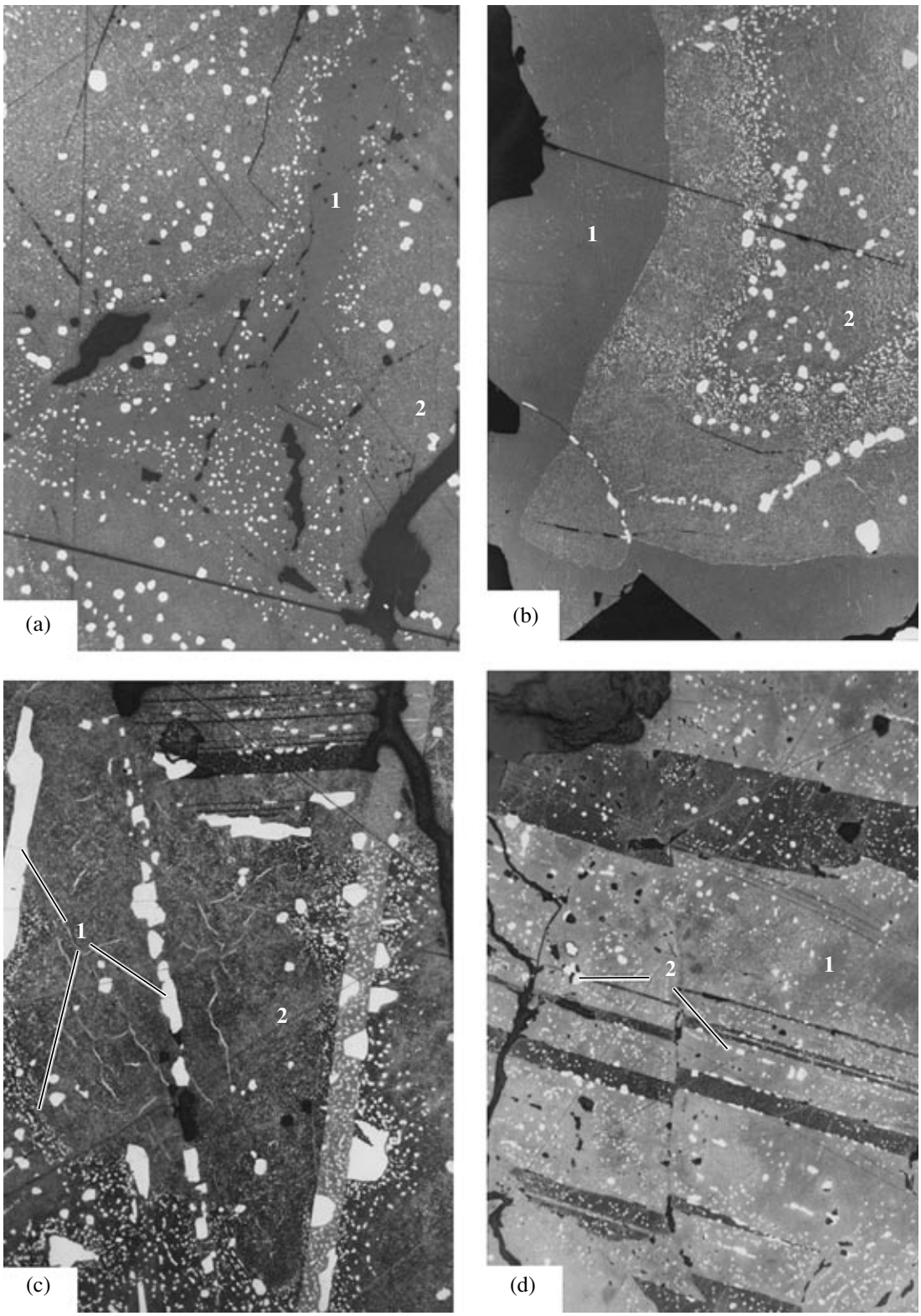

Fig. 4. Chalcopyrite inclusions in sphalerite of different generations. Polished sections. (b–d) Etched in aqua regia vapor. Magn. 100. (a) Veinlets of sphalerite II (1) that crosscut sphalerite I (2) with numerous chalcopyrite inclusions; (b) rim of redeposited sphalerite (1) around grains with numerous chalcopyrite inclusions (2) enlarged in the central part of the sphalerite grain and along the fractures; (c) distribution of varisized chalcopyrite inclusions (1) by twins and microfractures in sphalerite (2); (d) deformed sphalerite I (1) with chalcopyrite inclusions (2); displacement of twins and redistribution and growth of chalcopyrite grains near twins and fractures are observable.

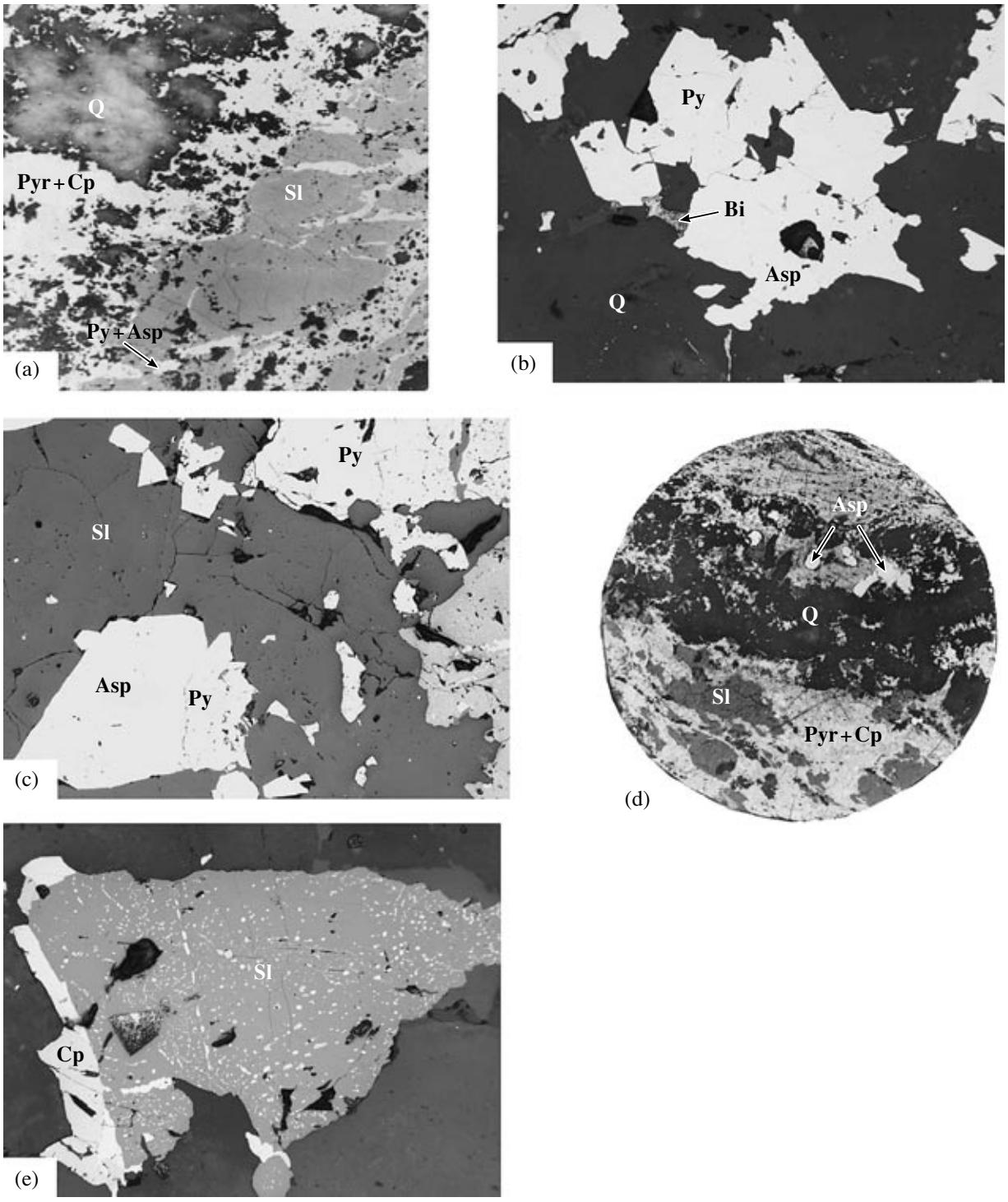

Fig. 5. Intergrowths of sulfide aggregates pertaining to the late mineral assemblages. Polished hand specimens and sections. (a) Chalcopyrite–pyrrhotite–sphalerite assemblage of the second stage; veinlets of pyrrhotite and chalcopyrite (Pyr + Cp) in sphalerite (Sl) are discernible; (b) pyrite–arsenopyrite aggregate (Py + Asp) in quartz (Q), small grain (Bi) is a bismuth mineral, magn. 100; (c) replacement of pyrite (Py) and arsenopyrite (Asp) with sphalerite (Sl), magn. 160; (d) stringer–disseminated chalcopyrite–sphalerite–pyrrhotite ore with the late arsenopyrite (Asp); relics of sphalerite (Sl) replaced by pyrrhotite (Pyr) and chalcopyrite (Cp) are discernible, natural size; (e) chalcopyrite (Cp) that grows over sphalerite (Sl) with numerous inclusions, magn. 160.

Table 2. Chemical composition of different sphalerite generations, wt %

Sample	Zn	Fe	S	Cu	Cd	In	Mn	Total
I generation								
D-99	53.74	13.1	32.32	0.043	0.15	0.008	0.58	99.94
D-322a	50.78	15.48	32.96	0.028	0.15	0	0.43	99.82
D-190	54.5	12.25	32.9	0	0.14	0	0.19	99.98
47-35	55.6	10.11	34.05	0.021	0.189	0.003	0.171	100.14
47-35	51.58	13.87	33.91	0.064	0.158	0	0.459	100.04
II generation								
D-93	61.56	5.84	32.57	0	0.19	0	0.04	100.2
D-93	60.37	6.51	32.58	0.023	0.22	0	0.29	99.99
D-322b	62.58	4.47	32.47	0	0.15	0.003	0.03	99.7
D-180	57.02	9.96	32.43	0	0.14	0.003	0.15	99.7
47-43	57.4	7.9	33.76	0	0.179	0.009	0.503	99.75
III generation								
D-98b	66.16	0.73	32.61	0.003	0.26	0	0.01	99.77
D-98a	66.11	0.97	32.54	0.009	0.24	0.007	0	99.87
47-19	64.16	1.94	33.59	0	0.211	0	0.006	99.9
47-21	63.28	2.96	33.31	0	0.177	0	0.012	99.73
47-52	62.58	3.88	33.55	0.006	0.18	0.003	0.074	100.27

reveal growth and pressure twins, which are occasionally displaced by late fractures (Fig. 4d), indicating a change of sphalerite structure during intramineral movements. Pyrrhotite that replaces sphalerite in the form of inclusions and veinlets is also noted together with chalcopyrite inclusions (Fig. 5a).

Three generations of sphalerite are recognized from crosscutting relations with other sulfides and gangue minerals.

Sphalerite I with chalcopyrite inclusions replaces pyrite I and arsenopyrite I and crosses these minerals as veinlets. Sphalerite II intergrows with pyrite, pyrrhotite, chalcopyrite, and occasionally galena. It contains pressure twins and is depurated from chalcopyrite inclusions (Fig. 4). Owing to recrystallization, regeneration, and redeposition, the sphalerite of this generation becomes heterogeneous in composition. Sphalerite III is often located at selvages, where it is commonly associated with galena and calcite. Sphalerite III is devoid of chalcopyrite inclusions or they are very rare. Inclusion-free sphalerite veinlets and rims around sphalerite II may be also ascribed to this generation (Figs. 4a, 4b).

The microprobe study (48 analyses) showed that sphalerites of different generations differ in major (Zn, Fe) and trace (Cd, Mn, In) element abundances (Table 2, Fig. 6).

Variations in Fe and Mn contents are most contrasting. In particular, sphalerite I is characterized by high Fe (>10 wt %) and Mn (up to 1.2 wt %) contents. Sphalerites II and III are significantly depleted in these elements: 4.5–9.9 and 0.7–3.9 wt % Fe, respectively, and no higher than 0.5 and 0.01–0.09 wt % Mn. The In and Cu contents decrease from the early to the late generations of sphalerite, whereas the Cd content increases in the same direction (Table 2, Fig. 6).

Judging from iron mole fractions, sphalerites analyzed with INAA (Table 3) represent all three generations. The microprobe (Table 2) and INAA determinations (Table 3) of Cd content are similar and demonstrate the same trend to enrichment of the late generations. The same tendency is observed for Co. Some sphalerites contain significant amounts of gold (up to 0.24 ppm); judging from the enrichment of these samples in As, the sphalerite concentrates are contaminated with Au-bearing arsenopyrite and/or arsenian pyrite. The relatively high Ag contents (up to 494 ppm) in sphalerite concentrates are presumably caused by contamination with Ag-bearing galena. It is notable that significant Se contents are detected in high-Ag samples.

Galena is the ore mineral second in abundance at the Dzhimidon deposit. It is widespread in the upper parts of orebodies, where locally it is prevalent over other ore minerals. Galena replaces pyrite, arsenopyrite, pyrrhotite, sphalerite, and chalcopyrite, corrodes their grains and aggregates, and fill dissolution cavities and fissures therein. In replacing sphalerite, galena often retains its relics but forms intergrowths with sphalerite III without indications of replacement. In local areas, all sulfides

except for galena bear signs of cataclasis. These observations indicate that the galena was deposited after the bulk of sulfides.

The chemical composition of galena is variable. The Bi and Ag contents vary depending on the level of orebody stripping. In the upper parts of orebodies, galena contains from 0.2 to 2.6 wt % Bi and up to 0.48 wt % Ag. Selenium is detected in some analyses. At deeper levels, in particular, in the East Dzhimidon ore zone, galena contains up to 14 wt % Bi and from 0.09 to 0.5 wt % Ag (Table 4). In these areas, galena typically occurs together with bismuth sulfosalts. Arsenopyrite, chalcopyrite, pyrrhotite, and marcasite are also noted.

The INAA determinations (Table 3) show that galena is the main Ag carrier at the Dzhimidon deposit, which is in accordance with microprobe results (Table 4). High contents of Se (up to 1051 ppm), Sb (up to 1079 ppm), and Au (0.69 ppm in one sample) have been detected. The latter sample is also enriched in Ag and Se.

Pyrite is widespread in ore and altered rocks, where it occurs as aggregates, granular segregations, veinlets, and metacrysts; close intergrowths with arsenopyrite are abundant (Fig. 5b). Three pyrite generations are distinguished: pyrite I as grains and aggregates that underwent deformation, cataclasis, fracturing, and brecciation (Fig. 7a); pyrite II, which forms veinlets crosscutting sphalerite, as well as metacrysts and metasomatic irregular aggregates in association with sphalerite and galena (Fig. 7b); and pyrite III intergrown with marcasite and occasionally with magnetite and siderite as a product of pyrrhotite saturation with sulfur.

As follows from the INAA results (Table 3), pyrite contains As (up to 8973 ppm), Co (up to 619 ppm), Au (0.13–0.51 ppm), and Se (up to 52 ppm).

Arsenopyrite is less abundant than sphalerite, galena, and pyrite but locally may be a major mineral, which is also represented by three generations. Arsenopyrite I occurs as euhedral, often brecciaed and deformed aggregates intergrown with pyrite I. Rhomboidal arsenopyrite II typically is associated with sphalerite, chalcopyrite, galena, quartz, and calcite (Fig. 5c), while arsenopyrite III overgrows fragments of these minerals, forming the cockarde structure.

The INAA results (Table 3) showed that arsenopyrite contains up to 64 ppm Au and is the main Au carrier at the Dzhimidon deposit. High Sb and notable Co contents were also detected.

Chalcopyrite often intergrows with sphalerite, pyrrhotite, and galena. As was mentioned above, chalcopyrite occurs as inclusions of variable shape and size in sphalerite I and II (Fig. 4). Two chalcopyrite generations are distinguished. Chalcopyrite I occurs as intergrowths with pyrrhotite I and sphalerite I. Chalcopyrite II is associated with galena and replaces and crosscuts sphalerite, corroding and overgrowing its aggregates. Chalcopyrite often contains relics of replaced sphalerite (Figs. 5a, 5d, 5e).

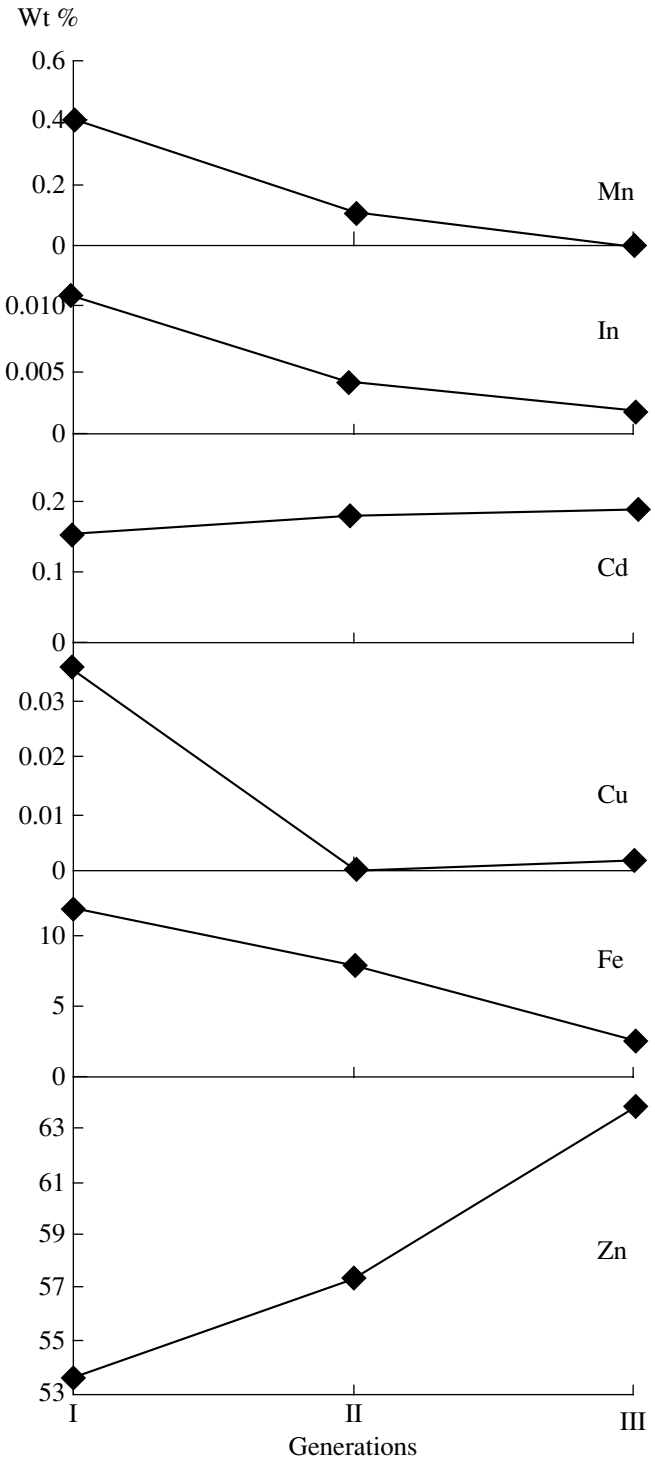

Fig. 6. Average trace element contents in sphalerite of different generations: I (24 analyses), II (9 analyses), and III (14 analyses).

Chalcopyrite contains Ag (up to 330 ppm) and Au (up to 0.2 ppm). The Cd contents, as in other sulfide concentrates, probably mark contamination with sphalerite. This is supported by the correlation between Cd and Zn (Table 3).

Table 3. Contents of elements, ppm in sulfide concentrates (INAA results)

Sample	Mineral	Fe	Co	Zn	As	Se	Ag	Cd	Sb	Au
47-9	Ap	351193	238.2	2607	220893	n.d.	n.d.	n.d.	5902	64.369
04/00	Py	460138	103.9	28	8973	11.1	3.2	″	13	0.509
07/00	″	496850	619.0	n.d.	486	51.7	n.d.	″	1	0.142
3-6	″	466358	38.2	11973	2128	5.6	4.1	38	16	0.249
3-8	″	417706	110.1	5652	3199	28.5	4.0	n.d.	11	0.343
47-4	″	392268	16.4	78309	1031	n.d.	17.4	169	22	0.202
47-6	″	427225	299.5	35670	2657	27.5	44.1	82	7	0.128
47-8	″	470528	596.2	n.d.	1559	22.7	n.d.	n.d.	3	0.448
3-2	Cp	322244	61.9	14460	963	6.5	330.3	43	14	0.188
3-8	″	293101	68.1	15967	174	14.6	43.9	71	3	0.044
47-3	″	282721	39.7	19736	217	6.1	104.0	78	5	n.d.
47-6	″	264352	127.0	43123	372	17.5	162.4	144	5	0.070
05/00	Gn	n.d.	n.d.	22	n.d.	90.6	1174.3	54	378	n.d.
06/00	″	687	n.d.	932	8	16.9	1183.6	n.d.	1079	″
3-2	″	3635	3.3	191	11	282.6	1516.5	19	160	″
3-6	″	1539	4.3	14523	3	102.7	1001.2	53	352	″
3-7	″	1192	1.8	6606	n.d.	24.9	376.8	24	353	″
3-8	″	636	2.5	5125	3	1051.1	3084.4	30	38	0.687
47-5	″	342	1.0	3081	n.d.	59.9	614.6	28	352	n.d.
06/00	Sp	120503	3.2	535095	n.d.	n.d.	n.d.	1213	3	n.d.
3-2	″	76418	101.2	562361	46	″	122.8	1433	5	0.140
3-3	″	66788	214.0	610794	2905	″	35.5	1586	27	0.109
3-6	″	55994	230.3	605728	172	″	91.5	1499	3	0.058
3-8	″	75514	152.3	473462	10	111.8	373.7	1245	2	0.243
47-2	″	33140	201.5	651161	n.d.	n.d.	n.d.	1725	n.d.	n.d.
47-4	″	94960	53.8	529395	23	″	38.6	1134	3	″
47-6	″	69106	206.9	494795	23	59.5	494.4	1320	1	″
47-7	″	56783	201.1	601961	n.d.	n.d.	n.d.	1533	n.d.	″

Note: (Ap) arsenopyrite, (Py) pyrite, (Cp) chalcopyrite, (Gn) galena, (Sp) sphalerite; n.d. is not detected.

Pyrrhotite occurs mainly at the lower levels of the deposit, where it is associated with pyrite I and arsenopyrite I. This pyrrhotite is referred to the first generation. Pyrrhotite I is often replaced by pyrite–marcasite and pyrite–magnetite–siderite aggregates, which testify to the elevated oxygen activity. Pyrrhotite II intergrows with sphalerite and chalcopyrite (Figs. 8a, 8b) and occasionally with galena; however, their temporal relations remain ambiguous. Pyrrhotite III occurs as elongated platy crystals in association with calcite, native bismuth, and bismuth sulfosalts (Figs. 8c, 8d).

The minerals considered below occur in subordinate amounts; however, many of them were identified at the deposit for the first time. Some of these minerals serve as concentrators of economic components.

Native silver was detected in the Bozang ore zone in association with knebelite, sphalerite, pyrite, and galena. Small (up to 10–15 μm in size) dendritic and rounded inclusions of native silver are hosted by chalcopyrite, which, in turn, is incorporated into sphalerite. The dendritic silver is devoid of impurities.

Acanthite was identified in samples from the Bozang ore zone as isolated elongated oval inclusions up to 150×60 μm in size hosted in chalcopyrite, which also contains fine sphalerite starlets. The chemical composition of acanthite is as follows (wt %): 83.7 Ag, 0.68 Cu, 0.64 Bi, 14.56 S, and 99.58 in total. The for-

Table 4. Chemical composition of bismuth minerals at the Dzhimidon deposit, wt %

No.	Sample	Pb	Bi	S	Fe	Ag	Sb	Se	Zn	As	Cu	Total	Mineral
1	3-8a	84.69	0.96	13.46	–	0.33	0.00	0.40	–	–	0.09	99.93	Galena
2	3-8a	84.43	1.35	13.37	–	0.46	0.00	0.47	–	–	0.02	100.10	″
3	1.8	70.24	14.09	13.91	0.06	0.30	0.00	0.28	–	–	0.07	98.95	Bi-galena
4	1.9	68.42	15.10	14.80	–	0.48	0.04	0.57	–	–	0.11	99.52	″
5	1.3	63.60	21.03	13.50	1.02	0.25	0.00	0.26	0.03	0.00	0.08	99.77	Beegerite
6	3-8a	60.63	24.07	15.05	–	0.95	0.01	0.51	–	–	0.00	101.22	$Pb_5Bi_2S_8$
7	1.3	59.06	26.89	11.05	0.34	2.00	0.09	0.26	0.05	0.00	0.00	99.74	Hungaryite
8	3-8a	53.62	30.17	15.39	–	0.65	0.03	0.50	–	–	0.40	100.76	$Pb_4Bi_2S_7$
9	1.1	50.86	34.84	13.50	0.09	0.43	0.00	0.23	0.04	0.00	0.00	99.99	Lillianite
10	3-8a	44.19	37.36	15.78	–	1.48	0.01	0.50	–	–	0.11	99.43	Bursaite
11	3-8a	39.68	42.36	16.28	–	0.75	0.01	0.25	–	–	0.61	99.22	″
12	3-8a	39.33	42.22	16.60	–	0.62	0.00	0.23	–	–	0.81	99.81	Cosalite
13	3-8a	39.28	42.69	16.41	–	0.68	0.00	0.15	–	–	0.79	100.00	″
14	1.6	37.86	44.91	15.42	0.09	0.25	0.04	0.20	0.04	0.00	0.00	98.81	″
15	2.2	37.58	42.26	15.97	1.18	1.64	0.21	0.11	0.03	0.01	0.51	99.50	″
16	47-43	37.58	44.74	15.28	–	2.63	–	–	–	–	–	100.24	″
17	2.1	36.73	40.86	16.07	4.03	1.69	0.11	0.11	0.00	0.00	0.49	100.09	″
18	47-43	34.68	47.61	15.58	–	1.90	0.00	0.10	–	–	0.30	99.35	Weibullite
19	47-43	33.78	48.04	16.70	–	1.30	0.00	0.10	–	–	0.00	100.16	″
20	47-43	32.31	47.76	15.97	–	5.60	0.00	0.10	–	–	0.40	98.24	$Ag_3Pb_8Bi_{11}S_{26}$
21	4	23.91	61.11	13.75	0.30	0.02	0.06	0.11	0.02	0.09	0.10	99.47	Galenobismutite
22	1.1	18.05	63.15	17.47	0.53	0.00	0.07	0.11	0.06	0.00	0.10	99.54	″
23	5	5.56	75.72	18.26	0.20	0.02	0.10	0.00	0.04	0.06	0.00	99.96	Bismuthinite
24	6.4	3.10	77.77	18.28	0.18	0.03	0.00	0.00	0.02	0.00	0.04	99.42	″
25	6.2	0.00	80.94	17.97	0.21	0.00	0.08	0.02	0.05	0.03	0.03	99.33	″
26	8.2	0.00	81.06	18.51	0.11	0.00	0.00	0.11	0.00	0.02	0.00	99.81	″
27	1.7	7.93	89.19	1.43	1.11	0.02	0.00	0.07	0.04	0.04	0.06	99.89	Native Bi
28	2.2	7.00	90.07	1.12	0.12	0.00	0.00	0.07	0.01	0.00	0.04	98.43	″
29	1	1.58	95.92	0.72	3.50	0.28	0.02	0.00	0.02	0.00	0.15	102.19	″
30	47-43	0.86	96.08	0.15	–	0.00	0.00	0.00	–	–	0.80	98.49	″
31	2.4	0.00	99.56	0.07	0.03	0.00	0.00	0.00	0.02	0.00	0.03	99.71	″
32	1.4	0.00	98.97	0.20	0.23	0.00	0.14	0.01	0.03	0.09	0.03	99.70	″
33	47-43	0.70	83.24	12.81	–	0.10	0.00	0.10	–	–	0.60	98.96	Bi_2S_2

Note: 47-43 and 3-8a are samples from the Bozang ore zone; other samples were taken from the East Dzhimidon ore zone; a dash denotes not analyzed.

mula calculated on the basis of three atoms is $[(Ag_{1.87}Cu_{0.03}Bi_{0.01})_{1.91}S_{1.09}]$.

The quartz–chlorite–feldspar aggregates in the East Dzhimidon ore zone often host discrete grains and aggregates of *scheelite* that contains (wt %) 14.54 Ca, 63.43 W, and 22.47 O. In altered rocks, scheelite is replaced by small wolframite crystals, which occasionally also occur independently of scheelite. The same samples contain sphalerite, galena, pyrite, organic matter, and K-feldspar. Since the tungsten minerals do not intergrow with sulfides, their relations with Pb–Zn mineralization remain unclear.

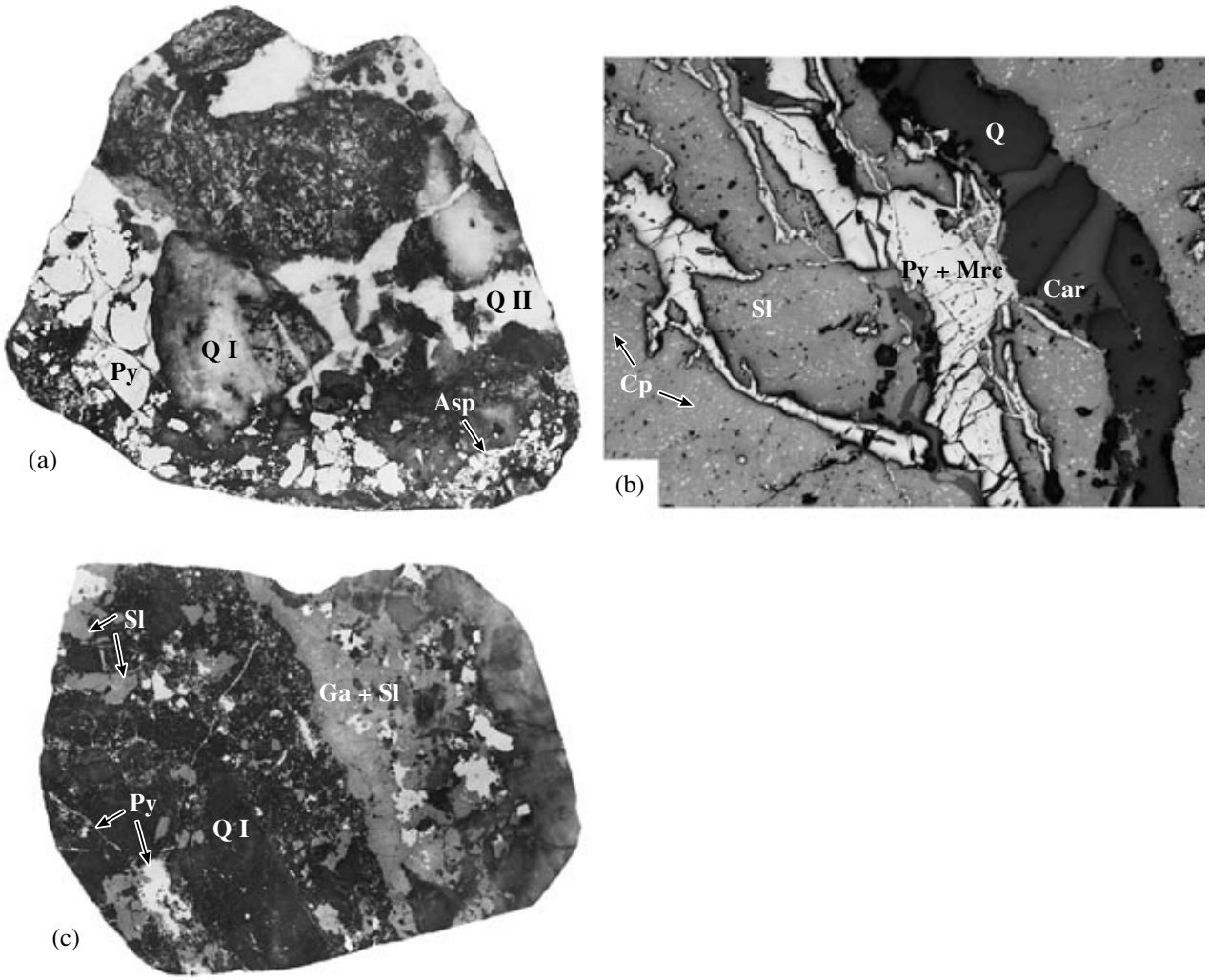

Fig. 7. Main structures and textures of the Dzhimidon ore. (1) Quartz–sulfide breccia, quartz I (QI) and quartz II (Q II) are brecciated and cemented with pyrite (Py) and arsenopyrite (Asp); fragments of crystalline schist (1) are seen, natural size; (b) late pyrite–marcasite (Py + Mrc) and quartz–carbonate (Q + Car) veinlets crosscut sphalerite (Sl) with dustlike chalcopyrite (Cp), magn. 160; (c) stringer–disseminated structure with brecciated early quartz (QI) on the left side of a hand specimen and with disseminations and veinlets of pyrite (Py), sphalerite (Sl), and galena (Ga) in interstices; galena–sphalerite (Ga + Sl) veinlet of the late mineral assemblage is seen on the right side, natural size.

Bismuth Mineralization

Bismuth mineralization in the Bozang and East Dzhimidon zones has been discovered at the Dzhimidon deposit for the first time. Aggregates and individual crystals of Bi-bearing minerals were detected in quartz; in calcite that replaced quartz (Figs. 9a–9c); and, less frequently, in pyrrhotite (Fig. 8b), arsenopyrite, sphalerite, and chalcopyrite. Discrete grains and their intergrowths vary from a few micrometers to tens of micrometers in size. The mineral grains are irregular, tabular, or acicular in shape and make up aggregates (Fig. 9).

The bismuth mineralization shows specific geochemical and compositional zoning. In particular, bismuth sulfosalts in the upper portions of orebodies (Bozang zone) are enriched in silver (up to 5.6 wt %); at the deeper levels (East Dzhimidon), the Ag content decreases to 1.7 wt %. Bismuthinite, abundant at a depth, gives way to cosalite at the upper levels. The bismuth minerals at the Dzhimidon deposit are closely associated with pyrite, arsenopyrite, and pyrrhotite. It is noteworthy that pyrrhotite in this association is transformed into disulfide. The bulk of bismuth minerals occurs within the depth interval from 180 to 220 m below the present-day surface, though their sporadic segregations were pointed out at a depth of ~100 m.

The most typical of 94 analyses of bismuth and Bi-bearing minerals given in Table 4 include Bi-bearing galena, beegerite, bursaite, weibullite, bismuthinite, native bismuth, hungaryite, cosalite, and lillianite, as well as previously unknown phases $Ag_3Pb_8Bi_{11}S_{26}$, Bi_2S_2, $Pb_5Bi_2S_8$, and $Pb_4Bi_2S_7$. Some of them are com-

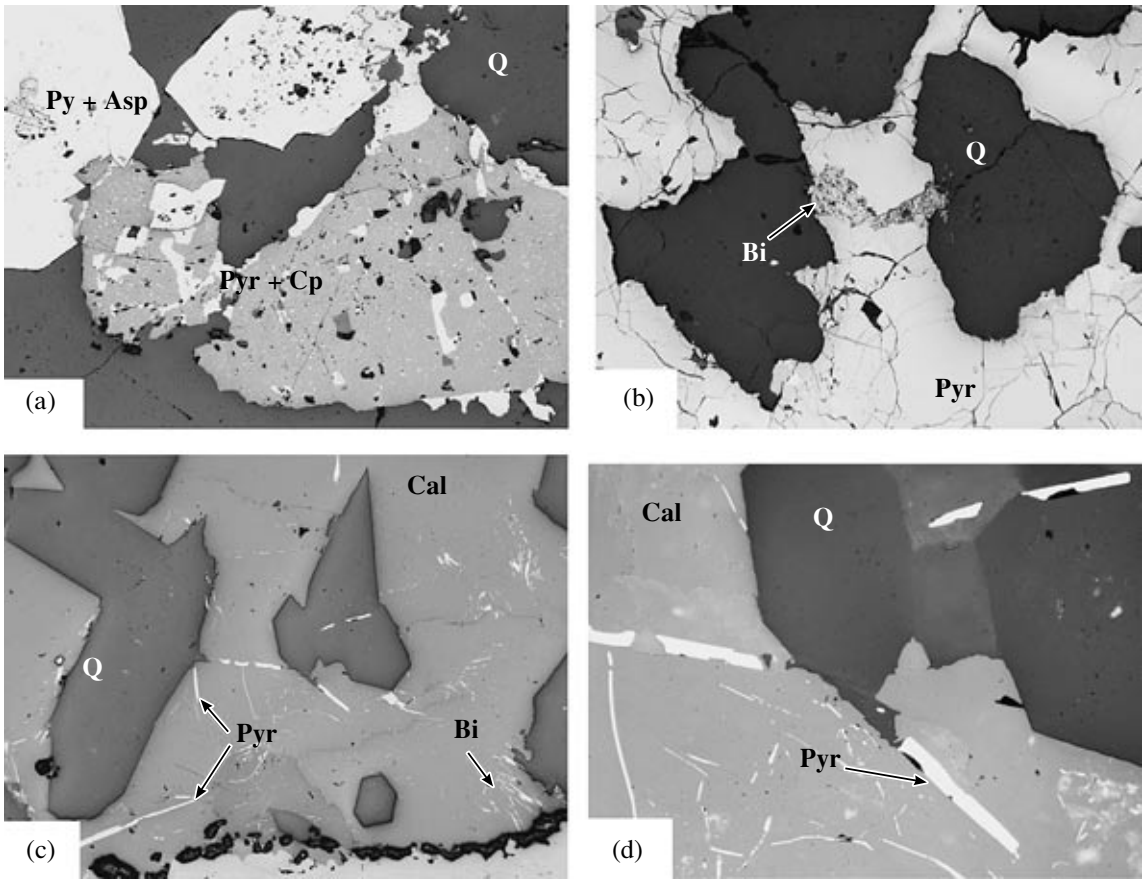

Fig. 8. Morphology of the late pyrrhotite. Polished sections, magn. 180. (a) Pyrrhotite aggregates with chalcopyrite inclusions (Pyr + Cp) in quartz (Q); pyrite and arsenopyrite crystals (Py + Asp) of the early stage are shown on the left side; (b) pyrrhotite (Pyr) with a veinlet of compositionally heterogeneous Bi-bearing mineral (Bi), quartz (Q) is dark; (c) platy aggregates of pyrrhotite (Pyr) in calcite (Cal) and quartz (Q); fine platelets and needles are a Bi mineral (Bi), quartz occurs as metacrysts in calcite; (d) close-up, magn. 200.

positionally similar to unnamed Pb and Bi sulfosalts previously described by Mozgova (1985).

Native bismuth was identified in samples taken from deep levels of the Bozang and East Dzhimidon ore zones. The mineral is closely related to aggregates of bismuth sulfosalts and occurs as individual small grains in quartz and carbonate (Figs. 8b, 9). Eight analyzed grains of native bismuth contain only traces of other elements except for one sample (Table 4, analysis 29) with appreciable amounts of Ag and Pb probably sourced from relics of Ag–Pb–Bi sulfosalts replaced by native bismuth.

Bismuthinite occurs as prismatic and acicular crystals and occasional fine-grained intergrowths in quartz (Fig. 9a) mainly at deep levels of the deposit. The bismuthinite (17 analyses) is very persistent in composition (75.7–83.2 wt % Bi and 15.8–18.4 wt % S). The bismuthinites depleted in Bi contain as much as 5.56 wt % Pb.

Cosalite is similar to bismuthinite in morphology (Fig. 9b); thin acicular crystals, sporadic intergrowths, and compacted aggregates are typical. Cosalite is optically heterogeneous and makes up intergrowths with other Bi-bearing minerals. The Bi content in cosalite increases with depth. The analyses of 17 cosalite grains are compositionally variable (wt %): 41.5–50.8 Bi, 36.6–41.2 Pb, 0.25–2.63 Ag, and 15.1–16.7 S.

Galenobismutite is virtually undistinguishable from cosalite in optic properties. These minerals are also close to each other in chemical composition, but galenobismutite is characterized by a higher Bi/Pb ratio.

Weibullite, bursaite, and Pb–Bi-bearing and Ag–Pb–Bi-bearing phases are significantly less abundant than the aforementioned minerals. They commonly occur as submicroscopic aggregates and intimate intergrowths with one another and are identified only from their chemical compositions (Table 4).

The chemical compositions of the studied bismuth minerals plotted on the phase diagram of the Pb–Bi–S system (Fig. 10) are grouped into two virtually continuous series. The series that extends from galena to bismuthinite and includes bismuthinite, bursaite, galena, and galenobismutite has been known for a long time and well studied experimentally (Craig, 1967). Some

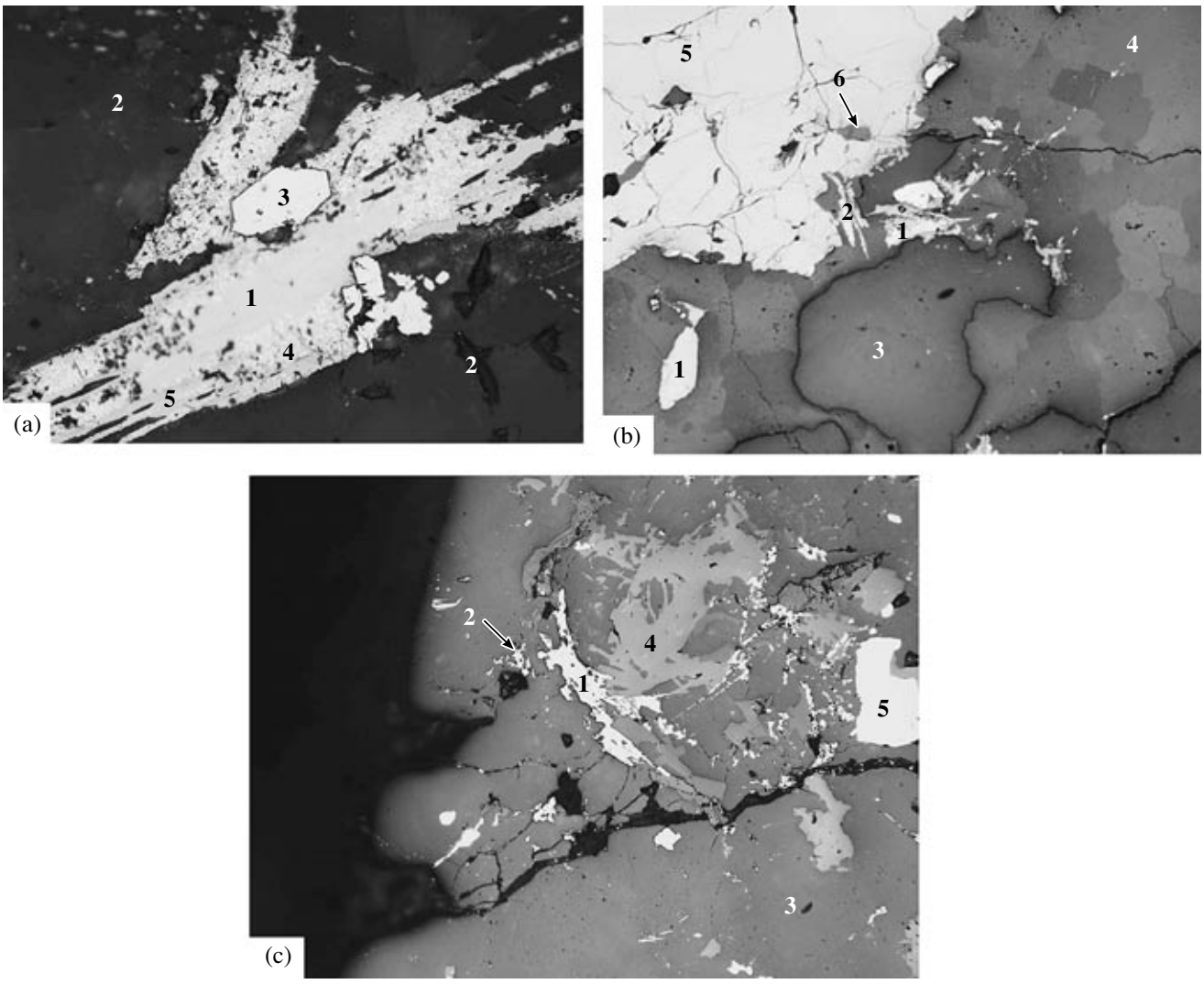

Fig. 9. Photomicrographs of Bi minerals and their intergrowths. Polished sections, magn. 250 (a), 160 (b, c). (a) Cosalite (1) in quartz (2) in association with late arsenopyrite (3); native Bi (4) (Table 4, an. 27, 32) and a heterogeneous phase (5) develop along cosalite margins (Table 4, an. 17); (b) tabular aggregates of bismuthinite (1) (Table 4, an. 23) and galenobismutite (2) (Table 4, an. 22) in quartz (3) and calcite (4) in association with arsenopyrite (5) and pyrrhotite (6); (c) aggregates of tabular bismuthinite (1) (Table 4, an. 27) and fibrous cosalite (2) (Table 4, an. 14) in quartz (3) and calcite (4); (5) chalcopyrite.

data points of minerals from the Dzhimidon deposit are clustered around theoretical compositions of known minerals in the PbS–Bi_2S_3 system, but a significant number of points are plotted both in the Pb-rich segment (between galena and bursaite) and in the Bi-rich segment (between galenobismutite and bismuthinite) of a nearly continuous series. The experimental study of this system (Craig, 1967) has shown that the appearance of natural phases with intermediate compositions may be attributed to their lower crystallization temperatures. As concerns the Dzhimidon ore, this possibility is supported by the results of fluid inclusion study, according to which the minerals under consideration crystallized at a lower temperature in comparison with that of the experimental study (400°C).

Some mineral phases are grouped into one more continuous series that extends from native bismuth to galena, revealing systematic variations in Pb and Bi proportions (Fig. 10). As was noted above, some mineral phases of this series are compositionally close to the poorly studied unnamed Pb–Bi sulfosalts mentioned in the monograph by Mozgova (1985).

Gangue Minerals

Quartz is the most abundant mineral of the ore. Its crystallization predated the deposition of Pb–Zn mineralization, accompanied ore deposition, and completed the formation of orebodies. Four quartz generations are distinguished. Quartz I, or Bozang quartz, is brecciated and broken. Quartz II crystallized together with pyrite I

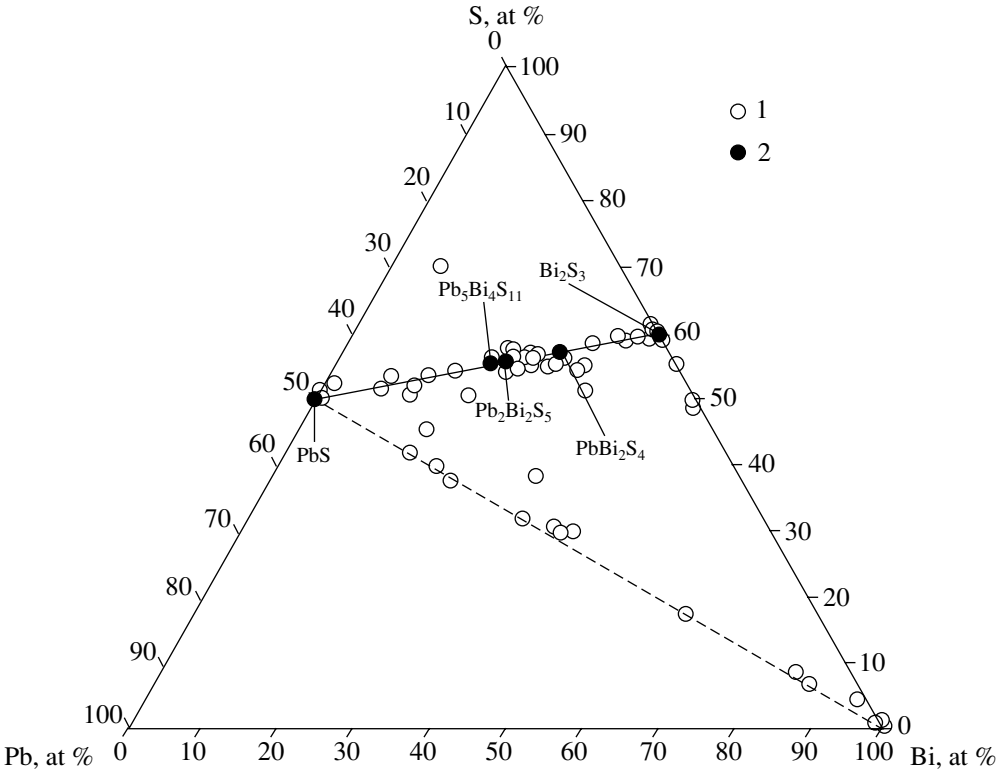

Fig. 10. Compositional variations of Bi minerals in the Bi–Pb–S system. (1) Minerals from the Dzhimidon deposit; (2) theoretical compositions.

and arsenopyrite I. Like the early sulfides, quartz II experienced deformation. Quartz III occurs as metacrysts in association with sphalerite, galena, and chalcopyrite. Quartz associated with Bi minerals was formed almost simultaneously with quartz III. Veinlets of quartz IV crosscut sulfides and altered wall rocks; quartz IV also occurs as small druses.

Chlorite I typically is abundant in selvages and products of wall rock alteration. Chlorite II as rosettes and relatively coarse-grained aggregates is associated with quartz II and III and sulfides. Chlorites I and II differ from each other in the Fe, Mg, Mn, and Ti contents. Chlorite I is enriched in Fe and Mn and contains traces of Ti. Chlorite II is commonly high-Mg, while the Fe content varies from one growth zone to another. A systematic change in iron mole fraction of chlorites from the Bozang zone was also mentioned by Konstantinov et al. (2004), who established that Fe-rich chlorite is confined to the ore zone, and Mg–Fe chlorites, to the supraore zone.

Carbonates at the Dzhimidon deposit are represented by predominant calcite and less abundant dolomite. In the ore, calcite is mainly associated with sphalerite II and galena. The late generations of calcite and quartz occur as crosscutting veinlets. Calcites are subdivided into manganese and ferruginous varieties. Dolomite and calcite are also observed in the deformed sulfide aggregates. Wide compositional variations were established in carbonates by microprobe analysis (wt %): 24.5–44.0 Ca, 0.17–12.4 Mg, 0.2–2.4 Fe, and 0.35–1.83 Mn.

Microcline was detected in the Bozang and East Dzhimidon ore zones as quartz–feldspar veins 30 cm thick. The mineral, which was identified by the chemical composition and X-ray pattern, is strongly deformed; chlorite and carbonate develop along the zones of microdeformation. Albite rims are occasionally seen at the boundary of chlorite and microcline. The microcline composition was determined with XRF as follows (wt %): 17.4 Al_2O_3, 66 SiO_2, 13.9 K_2O, 0.2 CaO, 0.2 Fe_2O_3, and 0.01 TiO_2. Insignificant amounts of S, F, Rb, Sr, Ba, and Cl were also detected. The X-ray diffraction pattern of microcline from the Dzhimidon deposit is similar to the reference pattern (PDF, no. 19-0932, 1966) in unit cell parameters: a = 8.497(4), b = 12.954(4), c = 7.185(3), α = 90.35(3), β = 116.63(4), γ = 88.07(4), and V = 706.5(4).

Knebelite. The samples from the Bozang ore zone, which were kindly supplied for the study by K.V. Davydov, were mainly composed of massive and sheaflike aggregates of a black mineral with distinct cleavage in separate crystals. Optical, chemical, and X-ray studies allowed its identification as knebelite. Elongated knebelite crystals occur in association with sphalerite, chalcopyrite, arsenopyrite, and galena. Occasionally, knebelite is surrounded by magnetite rims. The chemi-

cal compositions of two knebelite grains (wt %) are as follows: 31.01 and 31.00 Mn, 22.27 and 23.33 Fe, 0.73 and 0.67 Mg, 12.61 and 13.00 Si, 33.45 and 34.33 O, and 100.07 and 102.33 in total. The formulas calculated on the basis of seven atoms from the above compositions are $(Mn_{1.13}Fe_{0.80}Mg_{0.06})_{1.99}Si_{0.90}O_{4.17}$ and $(Mn_{1.10}Fe_{0.81}Mg_{0.05})_{1.96}Si_{0.90}O_{4.18}$, which is close to the knebelite formula. The X-ray powder diffraction pattern of the studied mineral (d_α, Å: 5.28, 3.99, 3.57, 3.075, 2.845, 2.665, 2.585, 2.526, 2.429, 2.330, 2.095, 1.934, 1.791, 1.720, 1.693, 1.666, 1.541, 1.530) also corresponds to the reference knebelite diffraction pattern (ASTM, no. 12-220, 1966).

STRUCTURAL AND TEXTURAL FEATURES OF THE ORE, MINERAL ASSEMBLAGES, AND THE SEQUENCE OF MINERAL FORMATION

The ores are massive, spotty, brecciated, banded, crustified, veined, and stringer–disseminated (Figs. 5, 7). These structures indicate that mineral aggregates were deposited by combined filling and replacement owing to variations in permeability.

Two types of brecciated ore are the most abundant at the deposit. The brecciated structure of the first type was formed as a result of cementation of host rock and quartz I fragments by quartz II and sulfides, mainly pyrite, arsenopyrite, and pyrrhotite (Fig. 7a). The second type is a sulfide breccia, where fragments of the early aggregates of iron sulfides, quartz, and sphalerite are cemented by chalcopyrite, galena, quartz, chlorite, and carbonate.

Ore veinlets and disseminated and spotty stringer ores are widespread at the deposit. They were formed by filling of fissures and interstices within veins (Figs. 7b, 7c). These structures are typical of both the early and the late mineral aggregates. In particular, pyrite and chalcopyrite veinlets are often observed in sphalerite. The late quartz and carbonate veinlets crosscut sulfide aggregates.

Central parts of orebodies are commonly spotty and massive. Highly variable proportions of arsenopyrite, galena, pyrite, sphalerite, and chalcopyrite are typical of these ores. The mineral species also vary from site to site, being represented either by pyrite and pyrrhotite; pyrite and arsenopyrite; or pyrrhotite, sphalerite, and chalcopyrite. The bismuth mineralization occurs locally.

The banded structure observed mainly in selvages demonstrates the opening and filling of near-contact fissures with sphalerite and associated minerals. The mineral aggregates of the banded ore often provide evidence for recrystallization, in particular, of sphalerite, as well as redistribution of chalcopyrite, pyrrhotite, and pyrite. The crustified ore with overgrowth structure occurs sporadically. Such ore is composed of late quartz–arsenopyrite aggregates (cockardes) growing over fragments of early quartz–sulfide aggregates.

Mineral grains and aggregates are diverse in textures. Chalcopyrite and pyrrhotite make up emulsion-like segregations, thin veinlets, and chains of grains hosted in sphalerite. Sphalerite starlets in chalcopyrite are not frequent. Pyrite, arsenopyrite, and quartz veinlets, as well as their metacrysts, may be observed in sphalerite, chalcopyrite, galena, and calcite. Central parts of orebodies exhibit various replacement and crosscutting relations. Indications of corrosion, relict grains, redeposition, recrystallization, and overgrowth are ubiquitous.

The ore formation sequence at the Dzhimidon deposit (Fig. 11) is confirmed by the study of the structural and textural features of ore and relationships between mineral aggregates. This sequence is consistent with the mineral formation stages previously established at other Pb–Zn deposits of the Sadon ore district, in particular, with those at the Arkhon deposit (Dobrovol'skaya, 1989). The sequence broadly corresponds to the evolution of the mineral-forming process in the Bozang ore zone outlined by Konstantinov et al. (2004) but significantly clarifies this process by recognizing compositionally different and sequentially formed mineral assemblages.

Five stages have been distinguished in the evolution of the Dzhimidon deposit: premineral (quartz–feldspar), first ore-forming (pyrite–arsenopyrite), second ore-forming (chalcopyrite–sphalerite), third ore-forming (arsenopyrite–sphalerite–galena), and postmineral (quartz–calcite). One or several mineral assemblages were deposited during each of these stages (Fig. 11).

The premineral stage was characterized by the formation of quartz, K-feldspar, chlorite, and sericite. Knebelite detected in xenoliths incorporated into the Pb–Zn ore was arbitrarily ascribed to this stage. Magnetite that replaced hematite and knebelite presumably also was formed at the premineral stage. Mineral aggregates of the earliest stage are in places fragmented, brecciated, and cemented by minerals of the quartz–pyrite–arsenopyrite assemblage of the first ore-forming stage.

The quartz–pyrite–arsenopyrite assemblage was formed during a period of tectonic activity. The mineral aggregates of this assemblage are represented by veinlets, spotty–veinlet segregations, or less frequently massive ore. Either pyrite or arsenopyrite dominates in the quartz–pyrite–arsenopyrite assemblage localized in different parts of orebodies (Fig. 5b); small amounts of sphalerite I are also noted. Quartz, pyrite, and arsenopyrite underwent cataclasis and are brecciated and fractured. The fractures are sealed with sphalerite II, chalcopyrite, galena, and quartz pertaining to the next mineral assemblage (Fig. 5c).

The minerals of the *quartz–galena–pyrrhotite–chalcopyrite–sphalerite assemblage*, which belongs to the second ore stage (Fig. 11, II), make up the bulk of the ore at the Dzhimidon deposit. Either pyrrhotite and chalcopyrite (Figs. 5a, 5d) or chalcopyrite, sphalerite II, and pyrite II (Fig. 5e) are prevalent in this assemblage

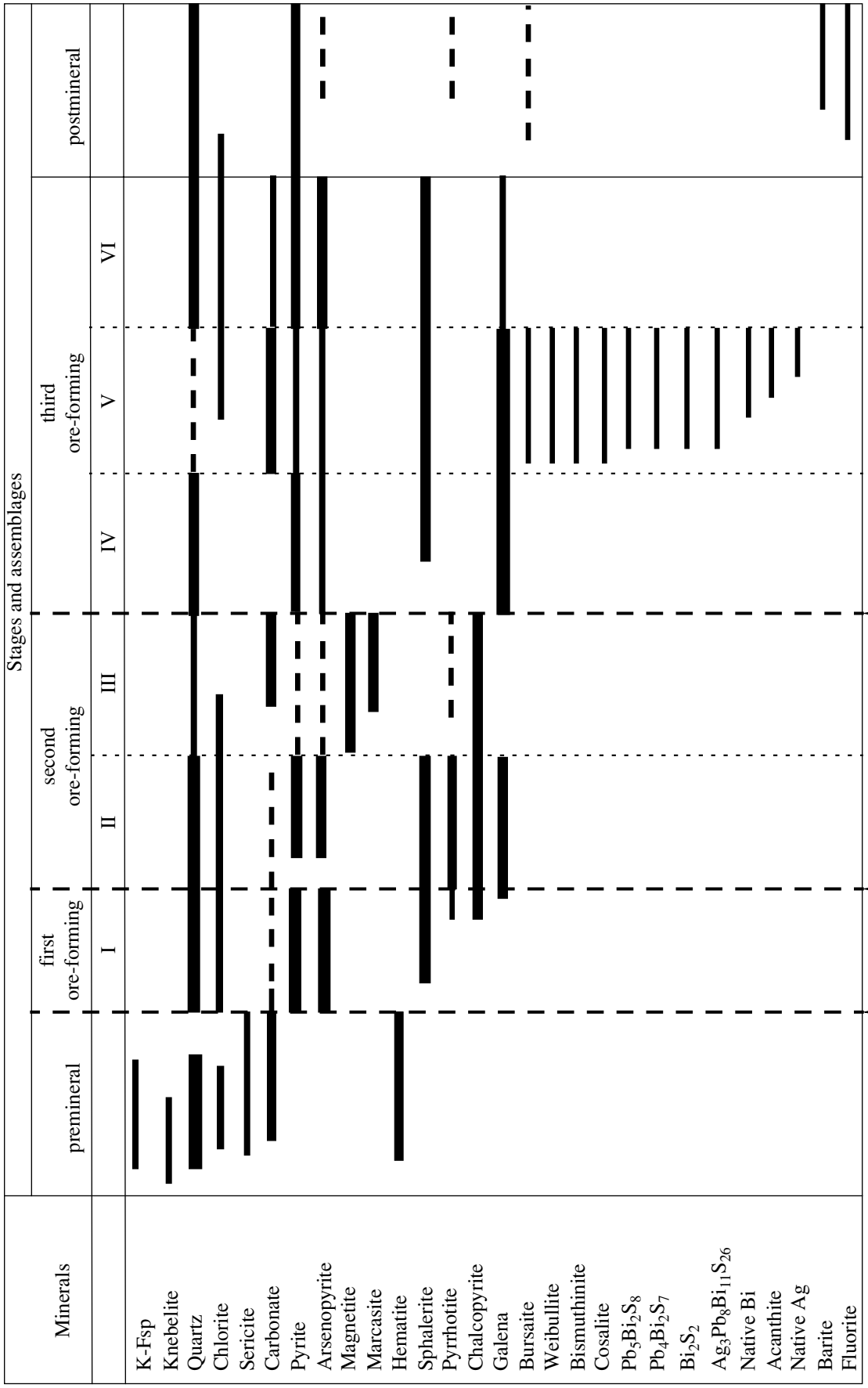

Fig. 11. Sequence of the mineral formation at the Dzhimidon deposit. (I–VI) Mineral assemblages: (I) quartz–pyrite–arsenopyrite, (II) quartz–galena–pyrrhotite–chalcopyrite–sphalerite, (III) carbonate–pyrite–marcasite–magnetite, (IV) quartz–chalcopyrite–galena–sphalerite, (V) bismuthinite–cosalite–galena, (VI) quartz–pyrite–arsenopyrite. (1–4) Minerals: (1) major, (2) minor, (3) accessory, (4) redeposited; (5) break.

from site to site. Curved and displaced twins in pyrrhotite and sphalerite, as well as local brecciation and boudinage of their aggregates, are revealed by etching. Galena was deposited later and bears no signs of deformation. Among minerals of this assemblage, sphalerite II is the earliest mineral, while magnetite II is one of the latest minerals, occurring as rims around sphalerite II or as small segregations in other sulfides. Quartz–sphalerite aggregates typically occur as veinlets or vein selvages.

The next, *carbonate–pyrite–marcasite–magnetite assemblage* (Fig. 11, III) is less widespread. It presumably was formed as a result of elevated sulfur and oxygen activities that led to the deposition of pyrite, marcasite, and in some cases magnetite III and siderite, which replaced pyrrhotite (saturation of iron disulfide with sulfur).

The third ore-forming stage comprises three mineral assemblages: quartz–chalcopyrite–galena–sphalerite (Fig. 11, IV), bismuthinite–cosalite–galena (V), and quartz–pyrite–arsenopyrite (VI). The *quartz–galena–chalcopyrite–sphalerite assemblage*, occasionally with additional calcite and pyrrhotite, occurs everywhere, being largely confined to the central parts of orebodies. It is noteworthy that pyrrhotite of this assemblage was not transformed into iron disulfide. Sphalerite III—a predominant mineral of the assemblage—occurs as intergrowths with galena, quartz, and calcite. Unlike sphalerite II, sphalerite III contains insignificant amounts of nonuniformly distributed and relatively large chalcopyrite inclusions. The *bismuthinite–cosalite–galena assemblage* occurs only locally. It is interesting that silver concentrates either in Ag–Pb–Bi–S sulfosalts associated with galena, native Bi, and Pb–Bi sulfosalts or in native silver and acanthite that accompany chalcopyrite and galena. The *quartz–pyrite–arsenopyrite assemblage* (Fig. 11, VI) of the third ore-forming stage is mainly represented by veinlets, where pyrite and marcasite occur as cockardes around quartz with sulfide disseminations and as metacrysts and fine streaks in sphalerite, chalcopyrite, and galena. Quartz metacrysts are often associated with the aforementioned sulfides.

The postmineral stage completes the formation of the Dzhimidon deposit. Quartz–calcite veinlets crossed the mineral aggregates of the preceding stages. Quartz dominates in some veinlets, while calcite is the major mineral in others. Some veinlets contain coarse-grained barite and colorless and greenish fluorite; both minerals fill cavities in druses. Quartz–fluorite–calcite–barite veins 20–30 cm thick are known beyond the main orebodies.

The newly obtained data and that available in the literature (Prokopenko, 1958; Dobrovol'skaya, 1987, 1989) characterizing the stages of mineral formation at the deposits of the Sadon ore district make it possible to outline some general features in the ore formation at these deposits, including the Dzhimidon deposit. The mineralization of the first ore-bearing quartz–arsenopyrite–pyrite stage has been established at all deposits of the Sadon ore district, while the second ore-forming chalcopyrite–sphalerite stage is developed only at the Arkhon and Kholst deposits. Ores of the Arkhon, Kholst, and Sadon deposits contain mineral assemblages of the third ore-bearing arsenopyrite–sphalerite–galena stage. Finally, the assemblages of the postmineral quartz–calcite stage complete the formation of all deposits in the Sadon ore district. Thus, the ore formation at all deposits of the Sadon ore district developed very similarly. The Arkhon deposit is the closest to the Dzhimidon deposit in composition of mineral assemblages and their sequence. The ore at the Verkhnii Zgid deposit is significantly enriched in manganosiderite and sphalerite in comparison with the Dzhimidon and other deposits of the Sadon ore district (Dobrovol'skaya, 1987, 1989).

PT FORMATION CONDITIONS OF THE DZHIMIDON DEPOSIT

Main Types of Fluid Inclusions

Primary and secondary fluid inclusions (FIs) have been studied in quartz of the premineral stage, in quartz and sphalerite of all three ore-forming stages, and in calcite of the postmineral stage. The classification of inclusions as primary or secondary was in line with known criteria (Roedder, 1984). The inclusions are 10–40 μm in size. They are divided into four types on the basis of the phase composition at room temperature.

Type 1 comprises two-phase fluid inclusions consisting of solution and a gas bubble that occupies ~30% of the vacuole volume (Figs. 12a–12c). Occasionally, the fluid inclusions contain a solid phase in the form of anisotropic elongated xenomorphic crystals, which are not dissolved by heating to 400°C and cannot be regarded as daughter minerals. The fluid inclusions of type 1, both primary and secondary, were revealed in quartz, sphalerite, and carbonate pertaining to all ore-forming stages.

The two-phase primary FIs of *type 2* were detected in quartz of the second and third ore-forming stages. They contain solution and a gas bubble that occupies 40–50% of the vacuole volume (Fig. 12d). In some inclusions, we were able to detect the appearance of liquid CO_2 on freezing; its melting on heating was observable in all inclusions.

Type 3 is represented by three-phase FIs. They contain solution and a gas bubble that occupies 40–50% of the volume and is rimmed by a thin film of liquid CO_2 (Fig. 12e). Inclusions of this type are primary and occur only in the quartz of the second ore-forming stage.

Type 4 comprises primary gas and substantially gas FIs with thin films of solution along the vacuole walls (Fig. 12f), which are syngenetic to the inclusions of types 2 and 3. They were revealed in quartz of the second and third ore-forming stages.

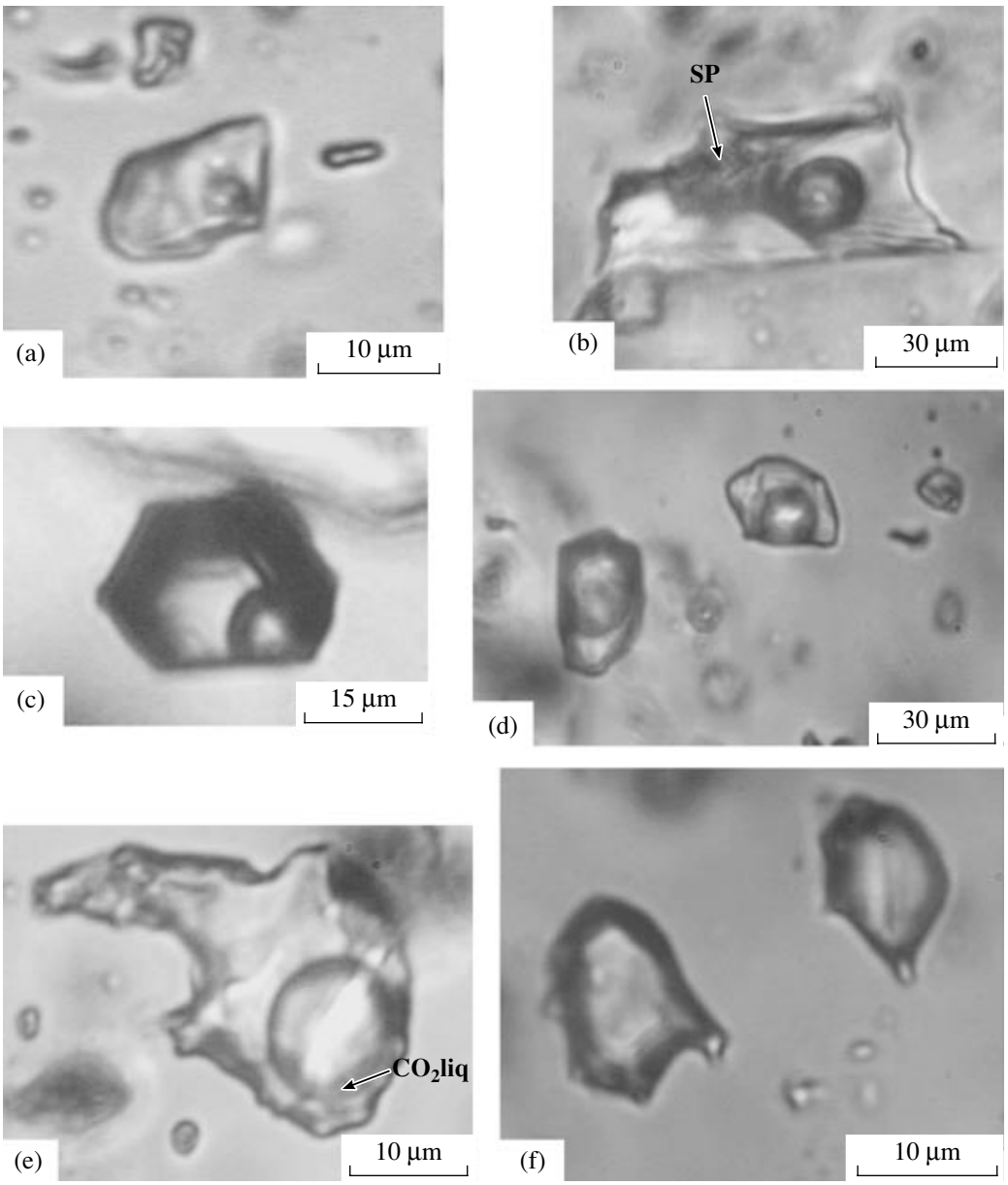

Fig. 12. Main types of fluid inclusions (FIs) in the minerals of the Dzhimidon deposit. (a) Type 1, secondary two-phase FIs in quartz; (b–f) primary fluid inclusions: (b) type 1, three–phase FIs (vapor + solution + solid phase) in quartz, (c) type 1, two-phase FIs in sphalerite, (d) type 2, two-phase FIs in quartz, (e) type 3, three-phase FIs (vapor + solution + CO_2liq) in quartz, (f) type 4, vapor-rich FIs in quartz. CO_2liq is liquid CO_2; (SP) insoluble solid phase.

Results of Fluid Inclusion Study

130 FIs in 11 samples representing all stages of the ore formation at the Dzhimidon deposit were involved in the microthermometric study; its results are summarized in Table 5.

The premineral stage. FIs were studied in quartz from the quartz–feldspar assemblage and from quartz–ore breccia, as well as in the Bozang quartz. Inclusions are mainly represented by type 2.

The primary inclusions (type 2) in quartz from breccia are filled with Na chloride solutions; T_{hom} ranges from 253 to 249°C and salinity, from 2.4 to 6.0 wt % NaCl equiv (Table 5). The inclusions froze to solid CO_2 and gas when cooled. CO_2 melted in the temperature range from –62.5 to –61.2°C and homogenized into the gas phase at 12–13°C. A decrease in T_{CO_2melt} indicates that CO_2 contains a significant admixture of CH_4 and other hydrocarbons. The secondary inclusions of type 1 (Fig. 12a) also contain Na chloride solutions with approximately the same salinity, ranging from 1.2 to 5.0 wt % NaCl equiv, but are devoid of CO_2; their T_{hom} is lower (150–138°C).

Table 5. Results of microthermometric study of fluid inclusions in minerals from the Dzhimidon deposit

Mineral, assemblage	*n*, (FI type)	T_{eut}, °C	T_{melt}, °C	Salinity, wt % NaCl equiv	T_{hom}, °C	T_{CO_2melt}, °C	$T_{clathrate\ melt}$, °C	T_{CO_2hom}, °C	*P*, bars
Premineral quartz–feldspar stage									
Quartz*	3 (p), type 2	–23.8…–24.5	–3.7…–1.4	6.0…2.4	253…249	–61.2…–62.5		13…12.1 V	
	7 (s), type 1	–21.8…–24.2	–3.0…–0.9	5.0…1.6	150…139				
Quartz**	9 (p), type 1	–21.3…–22.9	–6.0…–2.2	9.2…3.7	269…212				
The first ore-forming pyrite–arsenopyrite stage									
Quartz (I)	4 (p), type 2	–27.0…–28.1	–3.1…–2.0	5.1…3.4	323…300	–58.8…–62.0			
	5 (s), type 1	–27.7…–28.0	–5.8…–2.0	9.0…3.4	189…174				
Sphalerite (I)	8 (p), type 1	–28.3…–32.2	–7.5…–2.4	11.1…4.6	269…237				
The second ore-forming chalcopyrite–sphalerite stage									
Quartz (II)	6 (p), type 1	–23.9…–25.5	–7.0…–2.0	10.5…3.4	321…205				
	9 (p), types 2, 3	–23.0…–27.5	–5.5…–3.3	7.5…2.8	316…308	–58.5…–58.8	8.0…7.4	17.2…10.3 V	
	4 (p), type 4	–23.0	–5.5…–3.7	7.5…6.0		–58.1…–58.5		19.3…16.2 V	416…290
Quartz (III)	4 (p), type 1	–24.0…–27.0	–9.0…–8.0	12.9…11.7	202…185				
Sphalerite (III)	6 (p), type 1	–23.4…–27.1	–4.5…–2.1	7.2…3.6	200…190				
Quartz (III)	9 (p), type 1	–28.0…–31.6	–6.1…–0.2	9.2…0.4	194…152				
The third ore-forming sphalerite–galena stage									
Quartz (IV)	11 (p), type 1	–24.6…–32.7	–11.2…–1.2	15.2…2.1	343…171				
	6 (p), type 2	–35.0…–38.6	–13.3…–3.2	17.6…3.9	335…302	–58.3…–61.8	8.0…7.8	14.0…10.3 V	
	6 (p), type 4					–58.0…–60.5		27.8…17.5 V	426…300
Quartz (V)	6 (p), type 1	–37.0…–49.2	–19.8…–9.2	22.2…13.2	464…385				
Quartz (VI)	8 (p), type 1	–22.0…–27.4	–3.0…–0.8	5.0…1.4	164…118				
Quartz (VI)	7 (p), type 1	–25.6…–29.8	–2.7…–1.3	4.5…2.2	184…144				
Postmineral quartz–calcite stage									
Calcite	5 (p), type 1	–27.0…–28.7	–5.1…–2.4	8.0…4.0	237…221				

Note: *n* is the number of analyzed fluid inclusions: (p) primary, (s) secondary.
* Milky white quartz from breccia.
** Bozang quartz.

The Na chloride solutions in FIs (type 1) from the Bozang quartz have a relatively high salinity, from 3.7 to 9.2 wt % NaCl equiv. Their T_{hom} varies from 269 to 212°C. Unlike the primary FIs, the fluid inclusions in quartz from breccia do not contain CO_2.

The first ore-forming stage. Primary and secondary FIs were studied in quartz (types 1 and 2) and in sphalerite (type 1) from the quartz–pyrite–arsenopyrite–sphalerite assemblage (Fig. 11, I). The primary FIs (type 2) in quartz (Table 5, Fig. 12d) contain Na chloride solutions (T_{eut} varies from –27.1 to –28.1°C) with a salinity ranging from 3.4 to 5.1 wt % NaCl equiv and T_{hom} from 323 to 300°C. The fluid contains CO_2 with an admixture of methane and other hydrocarbons (T_{CO_2melt} varies from –58.8 to –62.0°C). CO_2 presumably homogenized in gas because we failed to determine its temperature. The freezing temperature of fluid inclusions testifies to a low CO_2 content. Judging by T_{eut} in the range from –28.3 to –32.2°C, the solutions of primary FIs in sphalerite contain Fe ions in addition to predominant Na^+. No CO_2 was detected in these fluids. The FIs have lower T_{hom} (269–237°C) and higher salinity (4.6–11.1 wt % NaCl equiv) than those in quartz.

The secondary FIs in quartz (type 1) also are Na chloride in composition but are distinguished by higher salinity, lower T_{hom} (Table 5), and the absence of CO_2.

The second ore-forming stage. FIs were studied in quartz and sphalerite from the quartz–galena–pyrrhotite–chalcopyrite–sphalerite (Fig. 11, II) and carbonate–pyrite–marcasite–magnetite (Fig. 11, III) mineral assemblages (Table 5). Quartz contains inclusions of all four types. FIs of type I contain Na chloride solutions with a salinity ranging from 3.4 to 10.5 wt % NaCl equiv, while T_{hom} varies in a wide range from 321 to 205°C (Fig. 12b). The inclusions of types 2 and 3 (Fig. 12e) also are Na chloride; however, they differ in narrower ranges of salinity (2.8–7.5 wt % NaCl equiv) and T_{hom} (316–300°C) as compared with FIs of type 1. CO_2 melted at a lower temperature (from –58.1 to –58.8°C) in comparison with pure CO_2, thus indicating an admixture of methane, and homogenized within the range 23.5–23.9°C. The inclusions contain Na chloride solutions with a salinity of 2.8–7.9 wt % NaCl equiv; T_{hom} varies from 316 to 307°C. Fluid in inclusions of type 4 (Fig. 12f) consists of predominant CO_2 and is heterogenized below room temperature; T_{melt} varies from –58.1 to –58.5°C and T_{hom} is 16.2–19.3°C.

The pressure was estimated at 290–416 bars. The calculation was performed for single-phase CO_2-bearing FIs at an average T_{hom} = 300°C. This pressure corresponds to the formation conditions of the quartz–galena–pyrrhotite–chalcopyrite–sphalerite assemblage and testifies to a relatively great depth of mineral formation at the beginning of the second ore-forming stage.

Quartz from the carbonate–pyrite–marcasite–magnetite assemblage contains FIs of type 1, which consist of Na chloride solution (T_{eut} ranges from –24.0 to –27.0°C) of elevated salinity (11.7–12.9 wt % NaCl equiv); the homogenization temperature varies from 185 to 201°C. Inclusions in sphalerite (Fig. 12c) also are Na chloride in composition and have similar T_{hom} (190–200°C); however, they differ by a lower salinity (7.2–3.6 wt % NaCl equiv). The later quartz that grew over sphalerite also contains FIs of type 1, which consist of Na chloride solution with T_{eut} = –(28.0–31.6)°C, a wider salinity range from 0.4 to 9.2 wt % NaCl equiv, and a lower T_{hom} of 152–194°C (Table 5).

The third ore-forming stage. FIs were studied in quartz from the quartz–chalcopyrite–galena–sphalerite (Fig. 11, IV), the bismuthinite–cosalite–galena (V), and the quartz–pyrite–arsenopyrite (VI) mineral assemblages (Table 5); FIs in sphalerite from assemblage (VI) were also studied. The coarse-grained quartz from the quartz–chalcopyrite–galena–sphalerite assemblage captured fluid inclusions of types 1, 2, and 4. Inclusions of type 1 contain Na chloride solutions with a salinity varying from 2.1 to 15.2 wt % NaCl equiv and T_{hom} from 171 to 343°C (Table 5). Unlike the inclusions of type 1, Mg^{2+} prevails among cations in chloride solutions in FIs of type 2; T_{eut} varies from –37.0 to –38.6°C and the range of T_{hom} is narrow (335–302°C). The salinity of the solution varies widely, from 17.6 to 3.9 wt % NaCl equiv (Table 5). These inclusions contain CO_2 with an admixture of CH_4 (T_{CO_2melt} varies from –58.3 to –61.8°C) (Table 5). Quartz from the same assemblage contains single-phase, substantially gaseous FIs of type 4, which are syngenetic to the inclusions of type 2. The cryometric data (T_{melt} = –(58.0–60.5)°C and T_{CO_2hom} = 17.5–27.8°C in gas) indicate that CO_2 contains a notable admixture of CH_4. The coexistence of two-phase gas–liquid CO_2-bearing inclusions and CO_2-rich FIs suggests that the quartz–chalcopyrite–galena–sphalerite assemblage was formed from a CO_2-saturated heterogeneous solution at a pressure from 300 to 426 bars, as calculated at the average T_{hom} (320°C) of two-phase inclusions that are syngenetic to the single-phase CO_2-bearing FIs. This pressure roughly corresponds to the estimated pressure at the beginning of the second ore-forming stage.

Fluid inclusions in quartz from the bismuthinite–cosalite–galena assemblage (type 1, Table 5) contain a mineral-forming solution with prevalent Mg^{2+} and other bivalent [LM1]ions as judged from T_{eut} = –(37.0–49.2°C). T_{hom} (464–385°C) and the salinity (22.1–38.5 wt % NaCl equiv) are the highest among all studied FIs. No CO_2 was detected by cryometric investigations.

FIs of type 1 were studied in quartz III and light sphalerite III from the quartz–pyrite–arsenopyrite assemblage (Fig. 11, VI). FIs in these minerals contain Na chloride solutions of approximately equal salinity (1.4–5.0 and 2.2–4.5 wt % NaCl equiv, respectively) and similar T_{hom} (118–164°C and 144–184°C, respectively).

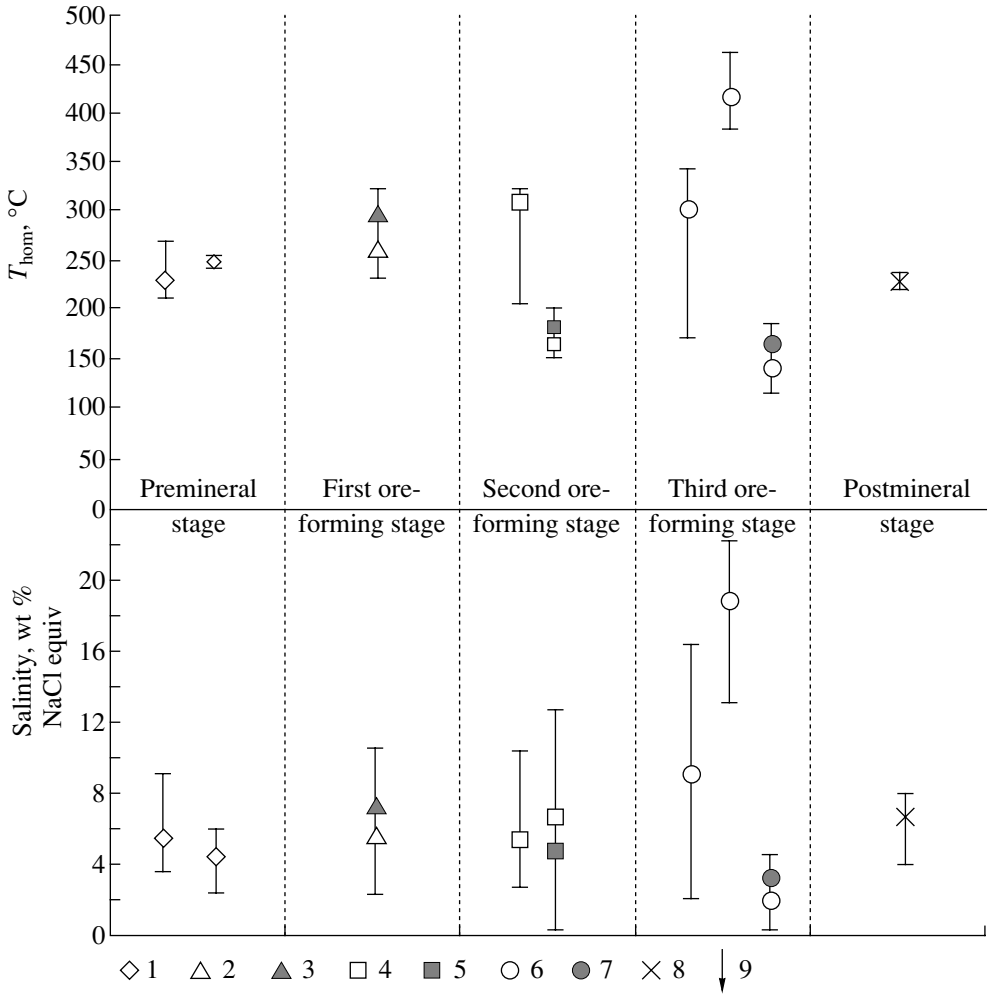

Fig. 13. Homogenization temperature and salinity of solutions (results of the study of fluid inclusions in minerals of the Dzhimidon deposit). (1) Quartz of the premineral stage; (2, 3) quartz and sphalerite of the first ore-forming stage; (4, 5) quartz and sphalerite of the second ore-forming stage; (6, 7) quartz and sphalerite of the third ore-forming stage; (8) calcite of the postmineral stage; (9) coexisting aqueous–salt and vapor inclusions.

The postmineral stage. FIs were studied only in calcite. They belong to type 1 and are two-phase (10% gas + solution). These FIs were found to homogenize in a narrow temperature range from 221 to 237°C and contain Na chloride solution with a moderate salinity (4.0–8.0 wt % NaCl equiv).

DISCUSSION

The mineral-forming fluids (Table 5) markedly varied in temperature, salinity, and composition during the multistage ore deposition at the Dzhimidon deposit (Figs. 13, 14). The mineral assemblages of the pre- and postmineral stages precipitated from medium-temperature solutions of moderate salinity (Table 5). The economic ore was formed from higher temperature and higher salinity solutions. At the beginning of the process, i.e., from the premineral to the first ore-forming stage and the beginning of the second stage, the temperature gradually increased and variations in salinity were insignificant. The onset of the third stage was marked by an abrupt increase in temperature and salinity of the ore-forming fluids and by widening of their ranges (Table 5, Fig. 13). It is noteworthy that the Na chloride composition of the mineral-forming solutions was retained from the premineral to the postmineral stage. Mg(Fe,Ca) chloride solutions participated in the formation of mineral assemblages only at the third ore-forming stage (Table 5, Fig. 14). This fact is worthy of special attention.

The diverse bismuth and silver minerals of the bismuthinite–cosalite–galena assemblage were formed at the third stage (Fig. 11). Among the gangue minerals, carbonates dominated over quartz; galena is enriched in Ag, Bi, and Se, and a low-Fe variety of sphalerite is predominant. These features distinguish this assemblage from other mineral assemblages. The circulation of

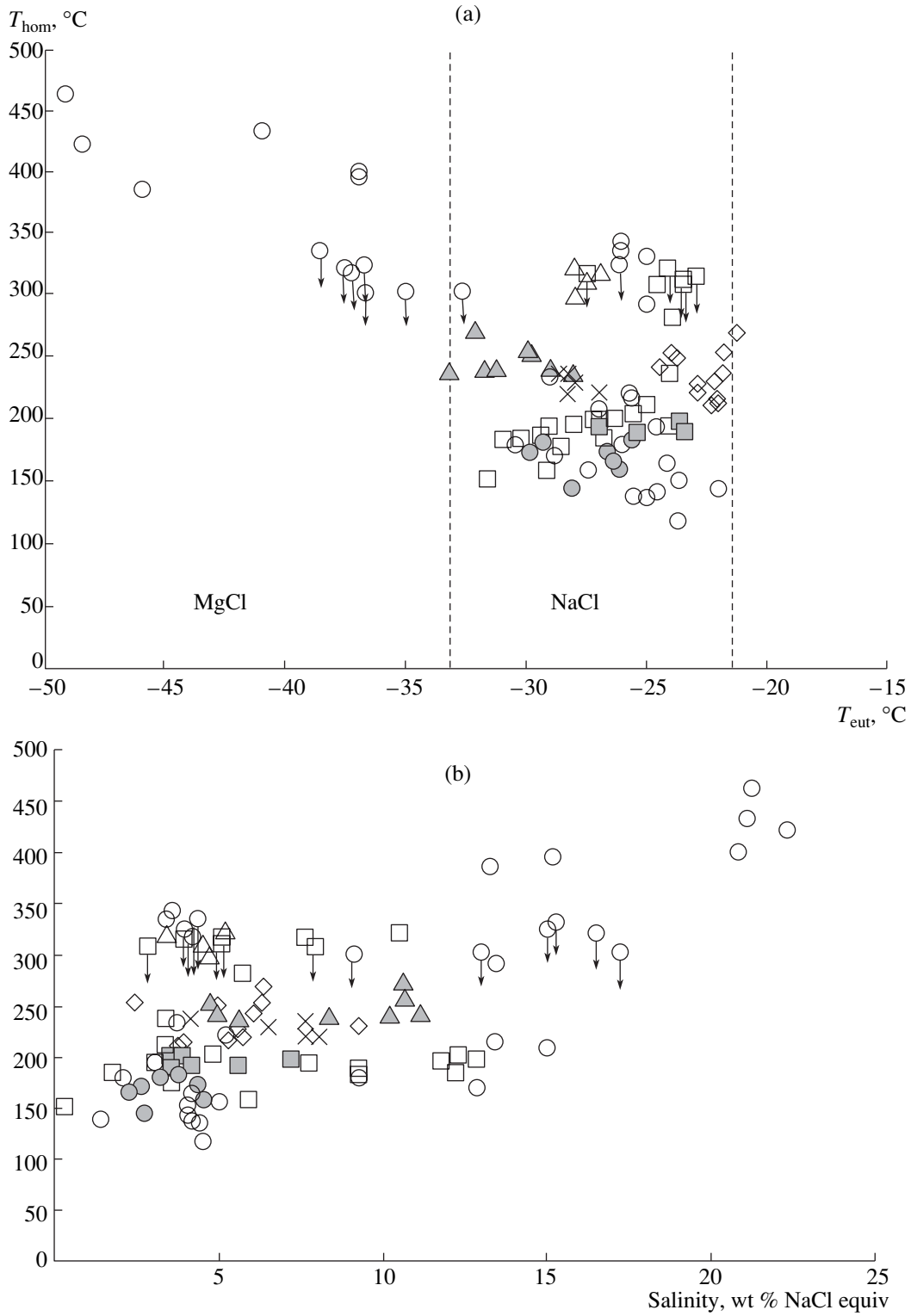

Fig. 14. (a) Homogenization temperature versus solution composition and (b) temperature versus salinity of the solutions (results of the study of FIs in minerals from the Dzhimidon deposit). See Fig. 13 for legend.

Mg(Fe,Ca) chloride fluids and the significant increase in temperature, which reached a maximum precisely during the deposition of the bismuthinite–cosalite–galena assemblage, suggest that a new source supplied high-temperature fluid to the hydrothermal system at the third ore-forming stage. The subvolcanic granite porphyry intrusions known in the ore field could be such a source.

The constant presence of carbon dioxide in fluids of all stages except the postmineral stage and a small admixture of CH_4 and probably other hydrocarbons are important features of the fluid regime that controlled the formation of mineral assemblages. An appreciable amount of CO_2 has been established in the fluids of the premineral stage. This amount decreased insignificantly at the first ore-forming stage and markedly increased during the ore deposition at the second and, especially, the third stages. The increase in salinity at the third stage presumably gave rise to the so-called salting out of CO_2 and led to the separation of an aqueous salt solution and a CO_2 gas phase. No indications of fluid boiling were recorded.

The pressure estimates for the second and third stages (416–290 and 426–300 bars, respectively; Table 5) may be spread over the entire multistage evolution of the Dzhimidon deposit. This statement is based on the results of cryometric study that confirmed the absence of liquid CO_2 in most studied inclusions and the homogenization of all CO_2-bearing FIs only in the gas phase. This implies that approximately the same pressure was maintained during the entire ore-forming process and this pressure did not exceed the calculated values.

CONCLUSIONS

(1) The mineral composition of Pb–Zn ore at the Dzhimidon deposit notably differs from that at other deposits of the Sadon ore district in a higher abundance of pyrite, arsenopyrite, chalcopyrite, native Bi and Ag, and Ag–Pb–Bi–S sulfosalts. In addition to bursaite, weibullite, bismuthinite, and cosalite, the sulfosalts include mineral phases of unusual compositions pertaining to two continuous series, PbS–Bi_2S_3 and PbS–Bi.

(2) The Pb–Zn ore at the Dzhimidon deposit is a product of multistage deposition, which began from quartz, K-feldspar, chlorite, sericite, carbonates, and hematite, occurring as veins, veinlets, disseminations, and breccias. The ore-forming process proceeded through three consecutive stages, when the economic orebodies were deposited. The mineral formation was completed by widespread quartz–calcite veins and veinlets, occasionally with barite, fluorite, pyrite, sphalerite (cleiophane), and galena.

(3) The ore-forming solutions were mainly Na chloride in composition during all the stages except the third ore-forming stage, when Mg(Fe,Ca) chlorides were also dissolved in the ore-forming fluids. The fluids contained CO_2 with a small admixture of CH_4 and other hydrocarbons except the postmineral stage. The temperature ranged from >460 to <120°C, and the salinity varied from >22 to <1 wt % NaCl equiv. These parameters changed from stage to stage. The most complex composition and the highest temperatures and salinities of the mineral-forming solutions at the third ore stage were related to the origination of a new high-temperature fluid source. Subvolcanic granite porphyry intrusions could have served as such a source.

ACKNOWLEDGMENTS

We are grateful to A.I. Tsepin, T.I. Golovanova, A.L. Kerzin, N.V. Trubkin, and A.I. Yakushev for the performance of analytical procedures. We thank E.I. Davydova and K.Ch. Tautieva for their assistance in collecting geological information and A.N. Krasnov for his assistance in computer drawing of illustrations. This work was supported by the Russian Foundation for Basic Research (project no. 04-05-64407) and carried out under the Institute of Geology of Ore Deposits, Petrography, Mineralogy, and Geochemistry project on the composition, structure, and formation conditions of ores at large endogenous deposits of noble and base metals.

REFERENCES

1. G. D. Azhgirei, "Exploration of Hidden Pb–Zn Deposits in Northern Osetia, Russia," Izv. Vyssh. Uchebn. Zaved., Geol. Razved., No. 4, 73–83 (1958).
2. E. F. Bashkina, "Tectonics and Zoning of the Zgid Deposit (Northern Osetia, Russia)," Geol. Rudn. Mestorozhd. **44** (3), 198–211 (2002) [Geol. Ore Deposits **44** (3), 160–187 (2002)].
3. R. J. Bodnar and M. O. Vitik, "Interpretation of Microthermometric Data for H_2O–NaCl Fluid Inclusions," in *Fluid Inclusions in Minerals: Methods and Application. Short Course of the Working Group "Inclusion in Minerals"* (Virginia Tech., Pontignano-Siena, 1994), pp. 13–17.
4. A. S. Borisenko, "Cryometric Analysis of the Salt Composition of Fluid Inclusions in Minerals," Geol. Geofiz. **18** (8), 16–27 (1977).
5. N. S. Bortnikov, A. D. Genkin, and M. G. Dobrovolskaya, "The Nature of Chalcopyrite Inclusions in Sphalerite: Exsolution, Coprecipital, or "Disease," Econ. Geol. **86**, 1070–1082 (1991).
6. P. E. Brown, "FLINCOR: A Fluid Inclusion Data Reduction and Exploration Program," in *Program with Abstracts of the Second Biennial Pan-American Conf. on Research on Fluid Inclusions* (1989), p. 14.
7. V. B. Chernitsyn, *Pb–Zn Metallogeny* (Naukova Dumka, Kiev, 1985) [in Russian].
8. S. F. Chernopyatov, "Relationship between Pyrrhotite and Base-Metal Mineralization in the Sadon Ore Field," Izv. Vyssh. Uchebn. Zaved., Ser. Tsvet. Metal., No. 4, 71–80 (1958).
9. J. R. Craig, "Phase Relations and Mineral Assemblages in the Ag–Bi–Pb–S System," Miner. Deposita **1** (4), 279–305 (1967).
10. K. V. Davydov and A. G. Granovsky, "New Data on Relationship between Base-Metal Ores in Mountainous Osetia with the Jurassic Volcanic–Plutonic Complex," Dokl. Akad. Nauk SSSR **282** (4), 941–945 (1985).
11. M. G. Dobrovol'skaya, "Mineralogical and Geochemical Criteria of Ore Mineralization Forecasting in the Sadon Ore Field," Izv. Akad. Nauk SSSR, Ser. Geol., No. 8, 92–102 (1987).

12. M. G. Dobrovol'skaya, *Lead–Zinc Ore Mineralization: Deposit types, Mineral Assemblages, Specific Features of Ore Deposition* (Nauka, Moscow, 1989) [in Russian].
13. A. G. Granovsky, "Thermobaric–Geochemical Zoning of Base-Metal Deposits in the Northern Caucasus," Geol. Rudn. Mestorozhd. **24** (6), 63–73 (1982).
14. A. G. Gurbanov and I. Arets, "Granites of the Late Paleozoic Diorite–Granite Association in the Northern Caucasus, Russia: Guides for Tungsten Mineralization," Petrologiya **4** (4), 386–406 (1996) [Petrology **4** (4), 362–380 (1996)].
15. A. G. Gurbanov and S. S. Zembatov, "Submeridional Impaired Zones and Their Role in Localization of Base-Metal Mineralization in Northern Osetia," Izv. Akad. Nauk SSSR, Ser. Geol., No. 5, 106–119 (1978).
16. G. V. Khetagurov and L. M. Katova, "Spatial Distribution and Origin of Base-Metal Ores in Mountainous Osetia," Sov. Geol., No. 9, 122–127 (1972).
17. V. A. Kalyuzhny, *Principles of the Theory of Mineral-Forming Fluids* (Naukova Dumka, Kiev, 1982) [in Russian].
18. M. M. Konstantinov, *Factors Guiding the Localization of Hidden Pb–Zn Mineralization in the Sadon Ore Belt* (Tr. TSNIGRI, Moscow, 1971), Vol. 99, pp. 189–197 [in Russian].
19. M. M. Konstantinov, V. T. Bitarov, N. P. Vargynina, et al., "Hidden Lead–Zinc Deposits of the Sadon Ore District: Discoveries and Prospects," Otech. Geol., No. 1, 31–36 (2003).
20. M. M. Konstantinov, Kh. Kh. Laipanov, N. P. Vargunina, et al., "The Bozang Lead–Zinc Deposit, Northern Osetia," Rudy Metal., No. 4, 33–48 (2004).
21. Yu. V. Lyakhov, K. M. Pozdeev, S. M. Tibilov, et al., "A Thermobaric–Geochemical Model of the Ore Zoning and Estimation of Resource Potential of the Sadon Pb–Zn District," Rudy Metal., No. 2, 45–54 (1994).
22. N. N. Mozgova, *Nonstoichiometry and Homologous Series of Sulfosalts* (Nauka, Moscow, 1985) [in Russian].
23. E. M. Nekrasov, *Structural Factors of Localization of lead–Zinc Vein Deposits* (Nedra, Moscow, 1980) [in Russian].
24. N. M. Prokopenko, *Mineralization Stages at the Lead–Zinc Deposits of the Sadon District* (Izd. Akad. Nauk SSSR, Moscow, 1958) [in Russian].
25. E. Roedder, *Fluid Inclusions in Minerals* (Reviews in Mineralogy, Mineral. Soc. Amer., 1984, Vol. 12; Mir, Moscow, 1987).
26. V. I. Sorokin, "Structure and Main Mineralization Stages of the Main Vein at the Verkhnii Zgid Deposit," Izv. Vyssh. Uchebn. Zaved., Ser. Tsvet. Metal., No. 1, 22–29 (1958).
27. T. Thiery, A. M. Van den Kerkhoff, and A. Dubessy, "V-X Modeling of CH_4–CO_2 and CO_2–N_2 Fluid Inclusion ($T < 31°C$, $P < 400$ bars)," Eur. J. Mineral. **6**, 773–781 (1994).
28. L. A. Vardanyants, "Metallogeny of the Caucasus," Izv. Akad. Nauk SSSR, Ser. Geol., No. 8, 145–162 (1933).
29. L. A. Vardanyants, *Mountainous Osetia in the Central Caucasus System* (Tr. TsNIGRI, Moscow, 1935), Vol. 29, pp. 25–27 [in Russian].
30. I. P. Zlatogurskaya, "Primary Zoning at the Zgid Base-Metal Deposit," Sov. Geol., No. 6, 37–41 (1958).
31. I. P. Zlatogurskaya, "Prospects of Deep-Seated Ore Mineralization at the Sadon and Zgid Base-Metal Deposits in the Northern Caucasus," Izv. Vyssh. Uchebn. Zaved., Ser. Geol. Razved., No. 3, 53–58 (1960).